IMA Journal of Numerical Analysis (2012) **32**, 1348–1374
doi:10.1093/imanum/drr041
Advance Access publication on January 17, 2012

Convergence analysis with parameter estimates for a reduced basis acoustic scattering T-matrix method

M. GANESH*
Department of Applied Mathematics and Statistics, Colorado School of Mines, Golden, CO 80401, USA
*Corresponding author: mganesh@mines.edu

S. C. HAWKINS
Department of Mathematics, Macquarie University, Sydney, NSW 2109, Australia
stuart.hawkins@mq.edu.au

AND

R. HIPTMAIR
Seminar für Angewandte Mathematik, ETH Zurich, CH-8092 Zürich, Switzerland
hiptmair@sam.math.ethz.ch

[Received on 30 January 2011; revised on 22 August 2011]

The celebrated truncated T-matrix method for wave propagation models belongs to a class of the reduced basis methods (RBMs), with the parameters being incident waves and incident directions. The T-matrix characterizes the scattering properties of the obstacles independent of the incident and receiver directions. In the T-matrix method the reduced set of basis functions for representation of the scattered field is constructed analytically, and hence, unlike other classes of the RBM, the T-matrix RBM avoids computationally intensive empirical construction of a reduced set of parameters and the associated basis set. However, establishing a convergence analysis and providing practical *a priori* estimates for reducing the number of basis functions in the T-matrix method has remained an open problem for several decades. In this work we solve this open problem for time-harmonic acoustic scattering in two and three dimensions. We numerically demonstrate the convergence analysis and the *a priori* parameter estimates for both point-source and plane-wave incident waves. Our approach can be used in conjunction with any numerical method for solving the forward wave propagation problem.

Keywords: wave propagation; acoustic scattering; T-matrix.

1. Introduction

The fast simulation of wave propagation induced by various types of incident waves impinging on a fixed bounded three-dimensional configuration (scatterer) from several directions is fundamental to several applications. In modern applications, the type of incident wave and associated incident and receiver directions are chosen by the end user, who requires certain online information quickly, while the shape of the configuration remains fixed (or based on a few prototype shapes). That is, the end users are given an infinite number of parameter options. The online requirements are typically functional outputs (such as the intensity or radar cross section) of mathematical models describing the wave propagation.

In such cases, independent of the user input, it is efficient to *a priori* construct and store certain information that completely characterizes (up to certain a certain accuracy) the essential scattering properties of the prototype configurations (using offline computations of appropriately discretized mathematical models) so that the online information can be simulated very quickly by the end users, for example, using simple matrix–vector multiplications, for any parameter choice. Here, the matrix describes the essential properties of the configuration and the vector is the input chosen by the end user.

In general, full mathematical models of physical processes contain some user input parameters. A framework that provides the end user with an infinite (online) choice of input parameters by first solving (offline) the full model for only a reduced, finite number of parameters is known as the reduced basis method (RBM) (see Afonso *et al.*, 2010; Pomplun & Schmidt, 2010; Chen *et al.*, 2010, 2011; Fares *et al.*, 2011; Patera & Rozza, 2011; Pomplun *et al.*, 2011; and extensive references therein for various applications). We refer to the methods discussed in these articles as the standard class of RBM and in this work we propose and analyse a new T-matrix class of RBM.

For a chosen application/model, the fundamental questions in the RBM are: (i) which choice of basis sets should be used to represent the functional outputs of the full models and the input functions (so that the output and input functions can be represented by vectors); (ii) how should a robust and practical *a priori* (or *a posteriori*) estimate of the cardinality of the reduced basis sets be provided; and (iii) how should a full convergence analysis of the associated RBM be established.

For the single-obstacle scattering wave propagation model considered in this work, the full set of parameters governing the model is the wavenumber, the type of incident wave and the incident and receiver directions. In this work we propose a new T-matrix class of exponentially converging RBM for time-harmonic acoustic scattering in two and three dimensions, with the user input parameters being the practically important types of incident wave:

(i) a plane wave with arbitrary incident direction;

(ii) the field generated by a point-source with arbitrary location;

and arbitrary receiver direction. The main aim of this work is to prove exponential convergence of the T-matrix RBM (with analytical representation of the reduced basis functions) and to establish a robust *a priori* analytical estimate for the reduced basis set.

The standard class of RBM has the advantage of allowing the wavenumber in the model to be a parameter as well. In this work we sacrifice this to gain the several advantages of the T-matrix class of RBM that are discussed below. In a future work, we shall consider a hybrid of the T-matrix class of RBM and a standard class of the RBM to include the wavenumber as a parameter and also allow configurations with multiple particles, following the recent work (Ganesh *et al.*, 2011) on the standard class of RBM.

The standard class of RBM requires an optimization method to select a reduced set of parameters and a computationally intensive construction of the reduced basis functions by solving the full model for all the selected offline parameters. The offline optimization procedure typically requires a fine discretization of the entire parameter domain and applies a greedy-type algorithm to select each offline snapshot parameter. The quality of the reduced basis set in the standard class of RBM depends strongly on the snapshot parameters chosen during the offline procedure. The choice of online parameters is restricted to the parameter domain used in the offline optimization procedure. For each choice of online parameter, the online procedure in the standard class of RBM requires simulation of the original model, but using the reduced basis. Efficient offline and fast online computations in the standard classes of the RBM require decomposition of the parameter and nonparameter variables in all the parameter-dependent input and output forms and functionals using approaches such as the empirical interpolation method (EIM) or

correlation matrix approaches such as the proper orthogonal decomposition (POD) or Karhunen–Loeve (KL) expansion methods.

We refer to recent literature (Pomplun & Schmidt, 2010; Chen *et al.*, 2010, 2011; Fares *et al.*, 2011; Ganesh *et al.*, 2011; Pomplun *et al.*, 2011) and references therein for some of the standard class of RBM for wave propagation models. Some of these articles also include error analysis and *a posteriori* estimates to choose the number of snapshot parameters, and hence the basis functions, empirically. Establishing robust analysis based *a posteriori* estimates and convergence analysis of the standard class of RBM still remains an active research area.

The T-matrix class of RBM in this work has several advantages compared to the standard class of RBM: firstly, an optimization-based procedure is not required to choose a reduced set of parameters. Arbitrary parameters can be chosen for online computation because the offline procedure does not use, or have any restriction on, the parameter domain. This is because the T-matrix is independent of the incident and receiver directions parameter set. Secondly, the offline reduced basis functions in the T-matrix class of RBM are constructed analytically. The offline procedure does not require a fine discretization of the parameter set and the use of greedy algorithms. Neither the offline nor the online procedures involve the use of decomposition approximations based on methods such as EIM/POD/KL. In our method, fast online computations can be carried out for any choice of input incident direction and output receiver direction without the need to solve the original model. The final online procedure requires only vector multiplication with the *a priori*-estimate-based truncated T-matrix to construct the required output signals.

In addition to proposing a new T-matrix class of RBM for practical types of incident waves, the fundamental strength of this work is in solving the several-decade-old problem of rigorously establishing exponential convergence of the method, with a concrete analytical *a priori* estimate on the number of reduced basis functions needed to achieve a desired accuracy. Our analysis also concretely shows that the number of reduced basis functions required for the truncated T-matrix approach is independent of the shape of the scatterer, which has been folklore in the T-matrix community but until now never proven. Our robust exponential convergence analysis and analytical representation of the *a priori* estimates are substantially different from those established for the standard class of RBM and may facilitate a new tool for future research in this active research area.

The T-matrix was first introduced for wave propagation over half a century ago in Waterman (1965) and the standard truncated T-matrix method has been widely used since then (see Doicu *et al.*, 2006); Martin, 2006; Mishchenko *et al.*, 1996, 2006; and the extensive references therein). The basis sets for the standard T-matrix method consist of the classical wave functions.

It is well known that the standard T-matrix method, which uses the null-field method, is numerically unstable and for large obstacles can become divergent (Mishchenko *et al.*, 1996, p. 543). There are several approaches to tackle this problem (Mishchenko *et al.*, 1996, 2006; Doicu *et al.*, 2006; Martin, 2006), such as using slow extended precision arithmetic to minimize the effect of round-off errors. The numerical instability arises mainly due to the use of near fields to compute entries in the reduced basis T-matrix and the fast growth of Hankel functions in the basis sets. In a recent work on acoustic scattering (Martin, 2006, Section 7.9.4), it was suggested that the instability could be avoided by using far fields, and the instability was computationally avoided in a robust way in Ganesh & Hawkins (2008, 2009) using the far fields of the Hankel functions. In these works convergence analysis was not addressed.

The standard T-matrix method has been investigated in the literature mainly for plane-wave incidence, with the end user supplied parameter being the arbitrary incident direction. Despite being widely used over the last five decades, it has been an open problem to establish a robust convergence analysis of any T-matrix method and to provide precise *a priori* parameter estimates to efficiently truncate the T-matrix, even for plane-wave incidence. While there have been several advances in the convergence

analysis and parameter estimates for several optimization-based RBMs (Afonso *et al.*, 2010; Patera & Rozza, 2011), the lack of a convergence analysis and parameter estimates for the optimization-free reduced basis T-matrix method has been considered a major disadvantage.

The main aim of this work is to avoid this major disadvantage by answering all three fundamental questions, for an optimization-free RBM with practically important point-source and plane-wave incidence with their source locations or wave directions as free user input parameters. In addition to providing *a priori* estimates for the truncation parameters and proving exponential convergence of the reduced basis T-matrix method, we demonstrate the theory and estimates using several numerical experiments for two- and three-dimensional acoustic scattering.

2. Acoustic obstacle scattering

In this section we describe in detail the model for acoustic obstacle scattering and the far-field pattern of the scattered field. We introduce index sets and various special functions from which we will, in Section 2.1, assemble a new class of regular and radiating functions.

We consider the model problem of time-harmonic exterior acoustic obstacle scattering in $\mathbb{R}^d$ for $d = 2, 3$. Let $D \subset \mathbb{R}^d$ be a bounded sound-soft, sound-hard or absorbing scatterer in a homogeneous medium. The coordinate system is chosen so that the origin $\mathbf{0}$ is inside D. Let $\rho_D > 0$ be the radius of the scatterer with respect to the origin, so that $D \subset B_{\rho_D}$, where $B_{\rho_D} \subset \mathbb{R}^d$ denotes the ball with centre $\mathbf{0}$ and radius ρ_D.

Let u^{inc} be an incident wave with wavelength $\lambda = 2\pi/k$, where k is the wavenumber, impinging on the scatterer D. The resulting time-harmonic radiating acoustic scattered-field u^{s} scattered by D satisfies the Helmholtz equation (Colton & Kress, 1998, Section 2.1),

$$\Delta u(\boldsymbol{x}) + k^2 u(\boldsymbol{x}) = 0\,, \quad \boldsymbol{x} \in \mathbb{R}^d \setminus \overline{D}\,, \tag{2.1}$$

and one of the following boundary conditions (properties of the scatterer):

$$u^{\text{s}}(\boldsymbol{x}) = -u^{\text{inc}}(\boldsymbol{x})\,, \qquad \text{(sound-soft)} \tag{2.2}$$

$$\frac{\partial u^{\text{s}}}{\partial \boldsymbol{n}}(\boldsymbol{x}) = -\frac{\partial u^{\text{inc}}}{\partial \boldsymbol{n}}(\boldsymbol{x})\,, \qquad \text{(sound-hard)} \tag{2.3}$$

$$u^{\text{s}}(\boldsymbol{x}) + \lambda \frac{\partial u^{\text{s}}}{\partial \boldsymbol{n}}(\boldsymbol{x}) = -u^{\text{inc}}(\boldsymbol{x}) - \lambda \frac{\partial u^{\text{inc}}}{d\boldsymbol{n}}(\boldsymbol{x})\,, \quad \operatorname{Im}(\lambda) > 0, \quad \text{(absorbing)} \tag{2.4}$$

for $\boldsymbol{x} \in \partial D$, and the Sommerfeld radiation condition

$$\lim_{|\boldsymbol{x}|\to\infty} |\boldsymbol{x}|^{(d-1)/2} \left(\frac{\partial u}{\partial |\boldsymbol{x}|} - \mathrm{i}ku \right) = 0, \tag{2.5}$$

where the limit holds uniformly in all directions $\widehat{\boldsymbol{x}} = \boldsymbol{x}/|\boldsymbol{x}| \in \mathbb{S}^{d-1}$, and $\mathbb{S}^{d-1}$ is the unit sphere in $\mathbb{R}^d$ for $d = 2, 3$. Furthermore, the radiating solution u^{s} has the asymptotic behaviour of an outgoing spherical wave (Colton & Kress, 1998, Theorem 2.5):

$$u^{\text{s}}(\boldsymbol{x}) = \frac{e^{\mathrm{i}k|\boldsymbol{x}|}}{|\boldsymbol{x}|^{(d-1)/2}} \left\{ u^{\infty}(\widehat{\boldsymbol{x}}) + \mathcal{O}\left(\frac{1}{|\boldsymbol{x}|}\right) \right\}, \tag{2.6}$$

as $|\boldsymbol{x}| \to \infty$ uniformly in all directions $\widehat{\boldsymbol{x}} = \boldsymbol{x}/|\boldsymbol{x}|$. The function u^∞ defined on $\mathbb{S}^{d-1}$ in (2.6) is known as the far-field pattern of u. Thus, the far-field $u^\infty \in L^2(\mathbb{S}^{d-1})$ has the representation

$$u^\infty(\widehat{\boldsymbol{x}}) = \lim_{|\boldsymbol{x}|\to\infty} |\boldsymbol{x}|^{(d-1)/2} e^{-\mathrm{i}k|\boldsymbol{x}|} u^{\mathrm{s}}(\boldsymbol{x}), \qquad \widehat{\boldsymbol{x}} = \boldsymbol{x}/|\boldsymbol{x}|. \tag{2.7}$$

Computation of the far-field pattern plays an important role in inverse scattering to identify the shape of the scatterer (Colton & Kress, 1998, Chapter 5).

For expansion of the incident, scattered and far fields using a new class of elementary regular and radiating functions and to unify notations in two and three dimensions, we introduce the infinite index sets

$$\mathbb{I}_d = \begin{cases} \{\boldsymbol{\ell} = \ell : \ell \in \mathbb{Z}\} & \text{for } d = 2, \\ \{\boldsymbol{\ell} = (\ell, j) : \ell \in \mathbb{N}_0, |j| \leqslant \ell\} & \text{for } d = 3, \end{cases}$$

and the finite subsets

$$\mathbb{I}_{d,N} = \begin{cases} \{\boldsymbol{\ell} = \ell : |\ell| \leqslant N\} & \text{for } d = 2, \\ \{\boldsymbol{\ell} = (\ell, j) : 0 \leqslant \ell \leqslant N, |j| \leqslant \ell\} & \text{for } d = 3, \end{cases}$$

where $\mathbb{N}_0 = \mathbb{N} \cup \{0\}$. For $\boldsymbol{\ell} \in \mathbb{I}_d$, with $\boldsymbol{\ell} = \ell$ or $\boldsymbol{\ell} = (\ell, j)$, we use the notation $|\boldsymbol{\ell}| = |\ell|$.

Let N_d denote the cardinality of $\mathbb{I}_{d,N}$. We have

$$N_d = \begin{cases} 2N + 1, & d = 2, \\ (N+1)^2, & d = 3. \end{cases} \tag{2.8}$$

Throughout the paper, for $\boldsymbol{\ell} \in \mathbb{I}_d$, the functions $J_{|\boldsymbol{\ell}|}$, $j_{|\boldsymbol{\ell}|}$, $H^{(1)}_{|\boldsymbol{\ell}|}$ and $h^{(1)}_{|\boldsymbol{\ell}|}$ are, respectively, the Bessel, spherical Bessel, Hankel and spherical Hankel functions of degree $|\boldsymbol{\ell}|$. For $\boldsymbol{\ell} = (\ell, j) \in \mathbb{I}_3$, we denote by $Y_{l,j}$ the spherical harmonic of degree l, given by

$$Y_{\ell,j}(\widehat{\boldsymbol{x}}) = (-1)^{(j+|j|)/2} \sqrt{\frac{2l+1}{4\pi} \frac{(l-|j|)!}{(l+|j|)!}} P_\ell^{|j|}(\cos\theta) e^{\mathrm{i}\, j\phi}, \qquad \widehat{\boldsymbol{x}} \in \mathbb{S}^2, \tag{2.9}$$

where $P_\ell^{|j|}$ is the associated Legendre function of degree ℓ and index j. Here we have used the spherical polar coordinate representation of the unit vector $\widehat{\boldsymbol{x}}$ with polar angle θ and azimuth ϕ. Formally, for $\boldsymbol{x} \in \mathbb{R}^2$ we write

$$\boldsymbol{x} = \boldsymbol{x}(\theta) = |\boldsymbol{x}|\widehat{\boldsymbol{x}} = |\boldsymbol{x}|(\cos\theta, \sin\theta)^{\mathrm{T}},$$

and for $\boldsymbol{x} \in \mathbb{R}^3$ we write

$$\boldsymbol{x} = \boldsymbol{x}(\theta, \phi) = |\boldsymbol{x}|\widehat{\boldsymbol{x}} = |\boldsymbol{x}|(\sin\theta\cos\phi, \sin\theta\sin\phi, \cos\theta)^{\mathrm{T}}.$$

We consider the orthonormal basis functions in $L^2(\mathbb{S}^{d-1})$ given by

$$Y_{\boldsymbol{\ell}}(\widehat{\boldsymbol{x}}) = \begin{cases} \frac{1}{\sqrt{2\pi}} \exp(\mathrm{i}\ell\theta), & d = 2, \\ Y_{\ell,j}(\widehat{\boldsymbol{x}}), & d = 3, \end{cases} \qquad \widehat{\boldsymbol{x}} \in \mathbb{S}^{d-1},\ \boldsymbol{\ell} \in \mathbb{I}_d. \tag{2.10}$$

In applications, the incident field u^{inc} is frequently an incident plane wave with propagation direction $\widehat{\boldsymbol{d}} \in \mathbb{S}^{d-1}$, and the far-field pattern u^∞ is the functional output of interest. In particular, one might like to know the acoustic cross section (ACS) of the scatterer at any user chosen direction $\widehat{\boldsymbol{x}} \in \mathbb{S}^{d-1}$, defined by

$$\sigma(\widehat{\boldsymbol{x}}; \widehat{\boldsymbol{d}}) = 4\pi\, |u^\infty(\widehat{\boldsymbol{x}})|^2. \tag{2.11}$$

A derived quantity of interest is the monostatic ACS, which is computed with $\widehat{\boldsymbol{d}} = -\widehat{\boldsymbol{x}}$. For the monostatic ACS , especially for nonconvex configurations, the full wave propagation model needs to be solved for thousands of incident directions $\widehat{\boldsymbol{d}}$ (representing the ACS from all directions). This requires a fast implementation of the far-field mapping $\widehat{\boldsymbol{d}} \mapsto u^\infty$. Another practically important class of incident waves is that of the circular and spherical waves generated by a point-source (located outside, but possibly close to, the configuration).

In this work, using a new class of basis functions, we first design an efficient offline computation to construct a matrix that is independent of the user input u^{inc} and that characterizes the scattering properties of the configuration pair $(\partial D, k)$ so that, given a user input u^{inc}, an approximate functional-output, the ACS, can be quickly computed online using cheap matrix–vector multiplication.

2.1 *Basis functions for expansion of fields*

In this section we introduce the new class of regular and radiating basis functions and derive L^2 norm bounds which we will use for the expansion and analysis of the incident and scattered fields in the obstacle scattering model.

The unknown quantity in the ACS formula (2.11) is the far-field u^∞. Using (2.6) and the orthonormal basis in (2.10), since the far-field $u^\infty \in L^2(\mathbb{S}^{d-1})$, there exists a sequence $\boldsymbol{a} = (a_{\boldsymbol{\ell}'})_{\boldsymbol{\ell}' \in \mathbb{I}_d}$ such that

$$u^\infty(\widehat{\boldsymbol{x}}) = \sum_{\boldsymbol{\ell}' \in \mathbb{I}_d} a_{\boldsymbol{\ell}'} Y_{\boldsymbol{\ell}'}(\widehat{\boldsymbol{x}}), \qquad \widehat{\boldsymbol{x}} \in \mathbb{S}^{d-1}. \tag{2.12}$$

An approximate far-field pattern can be obtained by truncating the expansion (2.12) to N_d' terms; that is, reducing the basis to N_d' functions. *A priori* error bounds may guide the choice of N_d' and to establish such bounds is the goal of this paper.

Hereafter, let $R > \rho_D$ be a fixed positive number to be read as the radius of a ball strictly containing D (see Figs 1, 11 and 12). The incident field u^{inc} satisfies the Helmholtz equation (2.1) everywhere inside B_R.

To motivate our approach, we first consider the incident field u^{inc} induced by a point-source located at $\boldsymbol{x}_0 \in \mathbb{R}^3$, with $|\boldsymbol{x}_0| > R$. Using Colton & Kress (1998, Theorem 2.10), we have the series representation

$$u^{\text{inc}}(\boldsymbol{x}) = \frac{\exp(\mathrm{i}k|\boldsymbol{x} - \boldsymbol{x}_0|)}{k|\boldsymbol{x} - \boldsymbol{x}_0|} = \sum_{\boldsymbol{\ell} \in \mathbb{I}_d} p_{\boldsymbol{\ell}}\; j_{|\boldsymbol{\ell}|}(k|\boldsymbol{x}|)\; Y_{\boldsymbol{\ell}}(\widehat{\boldsymbol{x}}), \tag{2.13}$$

with expansion coefficients

$$p_{\boldsymbol{\ell}} = 4\pi\,\mathrm{i}k\; h^{(1)}_{|\boldsymbol{\ell}|}(k|\boldsymbol{x}_0|)\; \overline{Y_{\boldsymbol{\ell}}(\widehat{\boldsymbol{x}}_0)}. \tag{2.14}$$

A similar expansion holds for any point-source radiation in two dimensions, using Graf's addition theorem (Abramowitz & Stegun, 1970, Equation (9.1.79)). Also, truncation to N_d terms, that is, those terms satisfying $|\ell| \leqslant N$, may be employed in (2.13).

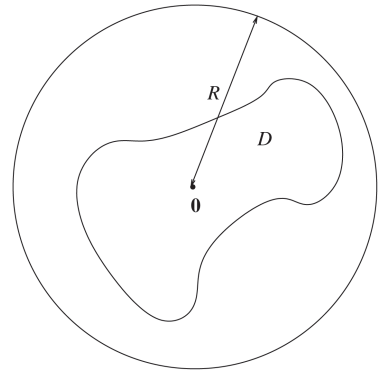

FIG. 1. Geometric arrangement for the acoustic scattering problem ($d = 2$).

In this article we provide a precise *a priori* bound for the error caused by the simultaneous truncation of (2.12) and (2.13). We establish exponential convergence of the resulting approximation error as both N' and N tend to ∞. Throughout the paper C stands for a generic positive constant, whose value may differ between different occurrences. The constant may depend only on the shape of D, the boundary conditions, the separation distance R and the wavenumber k. The constant does not depend on the truncation indices N and N' nor on the excitation u^{inc}.

After fixing N' and N, the offline task in this work is to compute an $N'_d \times N_d$ matrix so that the unknown reduced N'_d coefficients $a_{\boldsymbol{\ell}'}$ of the far field in (2.12) can be computed online using any N_d input incident field coefficients $p_{\boldsymbol{\ell}}$ via a matrix–vector product, which is typically cheap compared with the cost of solving the full model.

Motivated by (2.13), we introduce a new class of scaled elementary wave functions:

$$\widetilde{E}_{\boldsymbol{\ell}}(\boldsymbol{x}) = \begin{cases} H^{(1)}_{|\boldsymbol{\ell}|}(kR) J_{|\boldsymbol{\ell}|}(k|\boldsymbol{x}|) Y_{\boldsymbol{\ell}}(\widehat{\boldsymbol{x}}), & d = 2, \\ \\ h^{(1)}_{|\boldsymbol{\ell}|}(kR) j_{|\boldsymbol{\ell}|}(k|\boldsymbol{x}|) Y_{\boldsymbol{\ell}}(\widehat{\boldsymbol{x}}), & d = 3, \end{cases} \qquad \boldsymbol{\ell} \in \mathbb{I}_d. \tag{2.15}$$

The scaled wave functions are unbounded entire solutions of the Helmholtz equation (2.1) and can be regarded as 'incident circular/spherical waves'. The scaling factors applied to the usual regular wave functions are introduced in (2.15) to ensure boundedness of the coefficients in the incident field expansion for incident point-source waves. The waves (2.15) decay algebraically towards the origin.

LEMMA 2.1 With constants C depending only on D and kR,

$$\big\| \widetilde{E}_{\boldsymbol{\ell}} \restriction_{\partial D} \big\|_{L^2(\partial D)} \leqslant C \left(\frac{\rho_D}{R} \right)^{|\boldsymbol{\ell}|} \quad \forall \boldsymbol{\ell} \in \mathbb{I}_d, \tag{2.16}$$

$$\big\| \nabla \widetilde{E}_{\boldsymbol{\ell}} \restriction_{\partial D} \big\|_{L^2(\partial D)} \leqslant C \left(\frac{\rho_D}{R} \right)^{|\boldsymbol{\ell}|-1} |\boldsymbol{\ell}|^{d/2-1} \quad \forall \boldsymbol{\ell} \in \mathbb{I}_d,\ |\boldsymbol{\ell}| > 0. \tag{2.17}$$

Proof. We make use of the fact (Colton & Kress, 1998, Sections 2.4 and 3.4) that, with $C > 0$ depending on kR ,

$$\max \left\{ \big| H^{(1)}_{|\boldsymbol{\ell}|}(kR) J_{|\boldsymbol{\ell}|+\sigma}(kR) \big|, \big| h^{(1)}_{|\boldsymbol{\ell}|}(kR) j_{|\boldsymbol{\ell}|+\sigma}(kR) \big| \right\} \leqslant C |\boldsymbol{\ell}|^{\sigma-1} \quad \forall \boldsymbol{\ell} \in \mathbb{I}_d,$$
$$\sigma \in \{-1, 0, 1\}, \quad \sigma + |\boldsymbol{\ell}| \geqslant 0, \tag{2.18}$$

and of the estimate (see Colton & Kress, 1998, p. 31, for $d = 3$, and Equations (3.57) and (3.58), for $d = 2$)

$$\left|\frac{J_{|\boldsymbol{\ell}|}(k|\boldsymbol{x}|)}{J_{|\boldsymbol{\ell}|}(kR)}\right|, \left|\frac{j_{|\boldsymbol{\ell}|}(k|\boldsymbol{x}|)}{j_{|\boldsymbol{\ell}|}(kR)}\right| \leqslant C\left(\frac{|\boldsymbol{x}|}{R}\right)^{|\boldsymbol{\ell}|} \quad \forall \boldsymbol{\ell} \in \mathbb{I}_d,\ |\boldsymbol{x}| \leqslant R. \tag{2.19}$$

We combine this with (2.18) and the bound (see Freeden *et al.*, 1998, Lemma 3.1.5, for $d = 3$)

$$|Y_{\boldsymbol{\ell}}(\widehat{\boldsymbol{x}})| \leqslant C|\boldsymbol{\ell}|^{d/2-1}, \quad \widehat{\boldsymbol{x}} \in \mathbb{S}^{d-1}, \tag{2.20}$$

in (2.15) to obtain

$$|\widetilde{E}_{\boldsymbol{\ell}}(\boldsymbol{x})| \leqslant C\left(\frac{|\boldsymbol{x}|}{R}\right)^{|\boldsymbol{\ell}|} \quad \forall \boldsymbol{\ell} \in \mathbb{I}_d,\ |\boldsymbol{x}| < R, \tag{2.21}$$

which immediately yields the estimate for $\|\widetilde{E}_{\boldsymbol{\ell}}\restriction_{\partial D}\|_{L^2(\partial D)}$ in (2.16).

The proof of the second estimate starts from

$$\|\nabla \widetilde{E}_{\boldsymbol{\ell}}\restriction_{\partial D}\|_{L^2(\partial D)} \leqslant |\partial D|^{1/2}\,\|\nabla \widetilde{E}_{\boldsymbol{\ell}}\restriction_{\partial D}\|_{L^\infty(\partial D)}, \tag{2.22}$$

where $|\partial D|$ denotes the surface area of ∂D, and the polar/spherical coordinate representation for $|\boldsymbol{\ell}| > 0$,

$$\nabla \widetilde{E}_{\boldsymbol{\ell}}(\boldsymbol{x}) = \begin{cases} H^{(1)}_{|\boldsymbol{\ell}|}(kR)\big(kJ'_{|\boldsymbol{\ell}|}(k|\boldsymbol{x}|)Y_{\boldsymbol{\ell}}(\widehat{\boldsymbol{x}})\widehat{\boldsymbol{x}} + \frac{1}{|\boldsymbol{x}|}J_{|\boldsymbol{\ell}|}(k|\boldsymbol{x}|)\nabla^* Y_{\boldsymbol{\ell}}(\widehat{\boldsymbol{x}})\big), & d = 2, \\ h^{(1)}_{|\boldsymbol{\ell}|}\big(kR\big)(kj'_{|\boldsymbol{\ell}|}(k|\boldsymbol{x}|)Y_{\boldsymbol{\ell}}(\widehat{\boldsymbol{x}})\widehat{\boldsymbol{x}} + \frac{1}{|\boldsymbol{x}|}j_{|\boldsymbol{\ell}|}(k|\boldsymbol{x}|)\nabla^* Y_{\boldsymbol{\ell}}(\widehat{\boldsymbol{x}})\big), & d = 3, \end{cases} \tag{2.23}$$

where ∇^* is the surface gradient on $\mathbb{S}^{d-1}$. For $|\boldsymbol{\ell}| > 0$, using the formulas (Abramowitz & Stegun, 1970)

$$2J'_{|\boldsymbol{\ell}|} = J_{|\boldsymbol{\ell}|-1} - J_{|\boldsymbol{\ell}|+1}, \quad j_{|\boldsymbol{\ell}|}(t) = \sqrt{\frac{\pi}{2t}}J_{|\boldsymbol{\ell}|+1/2}(t),\ \ t \geqslant 0, \tag{2.24}$$

we get the surface gradient bound (see Freeden *et al.*, 1998, Lemma 12.6.7, for $d = 3$, and note the scaling term in Freeden *et al.*, 1998, Equation (12.2.1))

$$|\nabla^* Y_{\boldsymbol{\ell}}(\widehat{\boldsymbol{x}})| \leqslant C|\boldsymbol{\ell}|^{d/2}, \quad \widehat{\boldsymbol{x}} \in \mathbb{S}^{d-1}. \tag{2.25}$$

Substituting (2.18) and (2.19) in (2.23) yields the estimate

$$|\nabla \widetilde{E}_{\boldsymbol{\ell}}(\boldsymbol{x})| \leqslant C\left(\frac{\rho_D}{R}\right)^{|\boldsymbol{\ell}|-1}|\boldsymbol{\ell}|^{d/2-1} \qquad \forall \boldsymbol{\ell} \in \mathbb{I}_d,\ |\boldsymbol{\ell}| > 0,\ |\boldsymbol{x}| < R. \tag{2.26}$$

□

Using (2.15), we represent the incident wave u^{inc} as

$$u^{\mathrm{inc}} = \sum_{\boldsymbol{\ell} \in \mathbb{I}_d} p_{\boldsymbol{\ell}} \widetilde{E}_{\boldsymbol{\ell}}. \tag{2.27}$$

The details of such expansions and weights $p_{\boldsymbol{\ell}}$ for the physically important plane-wave and point-source incidence are discussed in Sections 3.1 and 3.2.

As with most error estimates, our truncation error bounds will depend on a measure of the 'smoothness' of the data, which is expressed through the requirement that suitable norms be bounded. Here, we assume that the incident wave u^{inc} with $u^{\mathrm{inc}}\restriction_{\partial D} \in L^2(\partial D)$ is such that there exists a weight sequence $\boldsymbol{w} = (w_{\boldsymbol{\ell}})_{\boldsymbol{\ell}\in\mathbb{I}_d}$ with

$$0 < \underline{w} \leqslant w_{\boldsymbol{\ell}} \quad \forall \boldsymbol{\ell} \in \mathbb{I}_d \quad \text{and some } \underline{w} > 0, \tag{2.28}$$

such that $u^{\mathrm{inc}} \in X_{\boldsymbol{w}}$, where

$$X_{\boldsymbol{w}} = \left\{ \psi = \sum_{\boldsymbol{\ell}\in\mathbb{I}_d} q_{\boldsymbol{\ell}} \widetilde{E}_{\boldsymbol{\ell}} : \|\psi\|^2_{X_{\boldsymbol{w}}} := \sum_{\boldsymbol{\ell}\in\mathbb{I}_d} w_{\boldsymbol{\ell}} |q_{\boldsymbol{\ell}}|^2 < \infty \right\}. \tag{2.29}$$

REMARK 2.2 Lemma 2.1 implies that for $u^{\mathrm{inc}} \in X_{\boldsymbol{w}}$, suitable restrictions of the expansion (2.27) converge in both $L^2(\partial D)$ and $L^2(B_R)$. From the estimates in the proof of Lemma 2.1 we also infer

$$X_{\boldsymbol{w}}\restriction_{B_R} \subset L^2(B_R) \quad \text{with continuous embedding.} \tag{2.30}$$

We also introduce a new class of scaled radiating waves

$$E_{\boldsymbol{\ell}}(\boldsymbol{x}) = \begin{cases} \dfrac{\sqrt{\pi k}}{(-\mathrm{i})^{|\boldsymbol{\ell}|}(1-\mathrm{i})} H^{(1)}_{|\boldsymbol{\ell}|}(k|\boldsymbol{x}|) Y_{\boldsymbol{\ell}}(\widehat{\boldsymbol{x}}), & d = 2, \\ \dfrac{k}{(-\mathrm{i})^{|\ell|+1}} h^{(1)}_{|\boldsymbol{\ell}|}(k|\boldsymbol{x}|) Y_{\boldsymbol{\ell}}(\widehat{\boldsymbol{x}}), & d = 3, \end{cases} \qquad \boldsymbol{\ell} \in \mathbb{I}_d. \tag{2.31}$$

The scaling factors in (2.31) are applied to the usual outgoing wave functions so that their associated far fields $\left\{E^{\infty}_{\boldsymbol{\ell}} : \boldsymbol{\ell} \in \mathbb{I}_d\right\}$ form an orthonormal basis for $L^2(\mathbb{S}^{d-1})$. In particular, using the asymptotics of the Hankel and spherical Hankel functions as $|\boldsymbol{x}| \to \infty$ (see Colton & Kress, 1998, Equations (3.59) and (2.41)) in (2.31), we get

$$E^{\infty}_{\boldsymbol{\ell}}(\widehat{\boldsymbol{x}}) = Y_{\boldsymbol{\ell}}(\widehat{\boldsymbol{x}}), \qquad \boldsymbol{\ell} \in \mathbb{I}_d,\ \widehat{\boldsymbol{x}} \in \mathbb{S}^{d-1},\ d = 2, 3. \tag{2.32}$$

Hence, using (2.12),

$$u^{\infty}(\widehat{\boldsymbol{x}}) = \sum_{\boldsymbol{\ell}'\in\mathbb{I}_d} a_{\boldsymbol{\ell}'} E^{\infty}_{\boldsymbol{\ell}'}(\widehat{\boldsymbol{x}}), \qquad \widehat{\boldsymbol{x}} \in \mathbb{S}^{d-1}. \tag{2.33}$$

In view of the above, it is natural to represent the radiating scattered-field u^{s} outside the ball B_R as

$$u^{\mathrm{s}}(\boldsymbol{x}) = \sum_{\boldsymbol{\ell}'\in\mathbb{I}_d} a_{\boldsymbol{\ell}'} E_{\boldsymbol{\ell}'}(\boldsymbol{x}), \qquad \boldsymbol{x} \in \mathbb{R}^d \setminus \overline{B}_R. \tag{2.34}$$

2.2 *Infinite basis: scattering matrix, far field, scattered field*

In this section we introduce the T-matrix, which connects the expansion coefficients of the incident and scattered fields. We briefly review a stable method for computing the T-matrix introduced by the authors in Ganesh & Hawkins (2008, 2009). This method avoids the numerical instability observed in the null-field method by using the far field rather than the near field for the T-matrix assembly.

We introduce bounded linear operators $S_\partial^\infty : Z(\partial D) \to L^2(\mathbb{S}^{d-1})$, where

$$Z(\partial D) := \begin{cases} H^{1/2}(\partial D) & \text{for a sound-soft scatterer (2.2),} \\ L^2(\partial D) & \text{for boundary conditions (2.3), (2.4).} \end{cases}$$

These operators map boundary data $g \in Z(\partial D)$ to the far-field pattern u^∞ of the solutions $u \in H^1_{\mathrm{loc}}(\mathbb{R}^d \setminus \overline{D})$ of the exterior boundary value problems[1]

$$\Delta u + k^2 u = 0 \qquad \text{in } \mathbb{R}^d \setminus \overline{D}, \qquad \begin{cases} u = g, & (2.35) \\ \text{or} & \\ \dfrac{\partial u}{\partial n} = g, \qquad \text{on } \partial D, & (2.36) \\ \text{or} & \\ u + \lambda \dfrac{\partial u}{\partial n} = g, & (2.37) \end{cases}$$

and the Sommerfeld radiation condition (2.5) at infinity. Continuity of S_∂^∞ follows from the estimates in Colton & Kress (1998, Section 2.5) and the fact that $u \in H^1_{\mathrm{loc}}(\mathbb{R}^d \setminus \overline{B}_R)$. Using S_∂^∞ we define the scattered-field operators $S^\infty : C^\infty(B_R) \mapsto L^2(\mathbb{S}^{d-1})$ as

$$S^\infty := S_\partial^\infty \circ B, \quad B\psi := \begin{cases} \psi \restriction \partial D & \text{for (2.35),} \\ \dfrac{\partial \psi}{\partial \boldsymbol{n}} \restriction \partial D & \text{for (2.36),} \\ \psi + \lambda \dfrac{\partial \psi}{\partial \boldsymbol{n}} \restriction \partial D & \text{for (2.37).} \end{cases} \tag{2.38}$$

Using (2.28) and the estimates of Lemma 2.1, we obtain that for u^{inc} the B-restrictions on the terms of the expansion (2.27) form sequences that converge in $Z(\partial D)$, which implies

$$S^\infty u^{\mathrm{inc}} = \sum_{\boldsymbol{\ell} \in \mathbb{I}_d} p_{\boldsymbol{\ell}} \left(S^\infty \widetilde{E}_{\boldsymbol{\ell}} \right) \quad \text{in } L^2(\mathbb{S}^{d-1}). \tag{2.39}$$

For each $\boldsymbol{\ell} \in \mathbb{I}_d$, since $S^\infty \widetilde{E}_{\boldsymbol{\ell}} \in L^2(\mathbb{S}^{d-1})$, there exists coefficients $t_{\boldsymbol{\ell}',\boldsymbol{\ell}}$ such that

$$\left(S^\infty \widetilde{E}_{\boldsymbol{\ell}} \right)(\widehat{\boldsymbol{x}}) = \sum_{\boldsymbol{\ell}' \in \mathbb{I}_d} t_{\boldsymbol{\ell}',\boldsymbol{\ell}} E^\infty_{\boldsymbol{\ell}'}(\widehat{\boldsymbol{x}}) = \sum_{\boldsymbol{\ell}' \in \mathbb{I}_d} t_{\boldsymbol{\ell}',\boldsymbol{\ell}} Y_{\boldsymbol{\ell}'}(\widehat{\boldsymbol{x}}), \qquad \widehat{\boldsymbol{x}} \in \mathbb{S}^{d-1}. \tag{2.40}$$

Using the orthonormality of the basis function in (2.10) with respect to the inner product $\langle \cdot, \cdot \rangle$ in $L^2(\mathbb{S}^{d-1})$, we get

$$t_{\boldsymbol{\ell}',\boldsymbol{\ell}} = \langle S^\infty \widetilde{E}_{\boldsymbol{\ell}}, Y_{\boldsymbol{\ell}'} \rangle, \qquad \boldsymbol{\ell}', \boldsymbol{\ell} \in \mathbb{I}_d. \tag{2.41}$$

[1] Of course, S_∂^∞ will be different for each boundary condition. For the sake of lean notation this dependence will be suppressed.

Using (2.40) in (2.39), we obtain

$$u^{\infty}(\widehat{\boldsymbol{x}}) = S^{\infty}u^{\mathrm{inc}}(\widehat{\boldsymbol{x}}) = \sum_{\boldsymbol{\ell}'\in\mathbb{I}_d}\left[\sum_{\boldsymbol{\ell}\in\mathbb{I}_d} t_{\boldsymbol{\ell}',\boldsymbol{\ell}}\,p_{\boldsymbol{\ell}}\right] E^{\infty}_{\boldsymbol{\ell}'}(\widehat{\boldsymbol{x}}), \qquad \widehat{\boldsymbol{x}}\in\mathbb{S}^{d-1}. \tag{2.42}$$

Comparing (2.42) with (2.33) shows that the incident field and the scattered/far-field coefficient sequences $\boldsymbol{p} = (p_{\boldsymbol{\ell}})_{\boldsymbol{\ell}\in\mathbb{I}_d}$ and $\boldsymbol{a} = (a_{\boldsymbol{\ell}})_{\boldsymbol{\ell}\in\mathbb{I}_d}$ are connected via the (infinite) T-matrix $T = \left[t_{\boldsymbol{\ell}',\boldsymbol{\ell}}\right]_{\boldsymbol{\ell}',\boldsymbol{\ell}\in\mathbb{I}_d}$ according to

$$\boldsymbol{a} = T\,\boldsymbol{p}. \tag{2.43}$$

2.3 *Reduced basis: scattering matrix, far field, scattered field*

Having described the infinite T-matrix in the previous section, we now discuss truncation of the T-matrix to obtain an algorithm that can be realized in practice. For a fixed pair of truncation parameters $N', N \in \mathbb{N}$, using the representation (2.41), we define the truncated $N'_d \times N_d$ reduced basis acoustic scattering T-matrix as

$$T_{N',N} = \left[t_{\boldsymbol{\ell}',\boldsymbol{\ell}}\right]_{\boldsymbol{\ell}'\in\mathbb{I}_{d,N'},\boldsymbol{\ell}\in\mathbb{I}_{d,N}}. \tag{2.44}$$

The $N'_d \times N_d$ truncated T-matrix can be precomputed and stored for any chosen scatterer, independent of the incident wave. Using the representation of u^{inc} in (2.27) and the associated truncated vector $\boldsymbol{p}^{(N)} = (p_{\boldsymbol{\ell}})_{\boldsymbol{\ell}\in\mathbb{I}_{d,N}}$ (which is known analytically for the physically important plane-wave and point-source incident waves), we can compute the vector $\boldsymbol{a}^{(N',N)} = \left(a^{(N',N)}_{\boldsymbol{\ell}'}\right)_{\boldsymbol{\ell}'\in\mathbb{I}'_{d,N}}$ using

$$\boldsymbol{a}^{(N',N)} = T_{N',N}\,\boldsymbol{p}^{(N)}. \tag{2.45}$$

In particular, using (2.33)–(2.42), for an incident field u^{inc} with representation (2.27), our approximation to the induced far field is

$$u^{\infty}_{(N',N)} = \sum_{\boldsymbol{\ell}'\in\mathbb{I}_{d,N'}}\left[\sum_{\boldsymbol{\ell}\in\mathbb{I}_{d,N}} t_{\boldsymbol{\ell}',\boldsymbol{\ell}}\,p_{\boldsymbol{\ell}}\right] E^{\infty}_{\boldsymbol{\ell}'} = \sum_{\boldsymbol{\ell}'\in\mathbb{I}_{d,N'}}\left[\sum_{\boldsymbol{\ell}\in\mathbb{I}_{d,N}} t_{\boldsymbol{\ell}',\boldsymbol{\ell}}\,p_{\boldsymbol{\ell}}\right] Y_{\boldsymbol{\ell}'}. \tag{2.46}$$

Our approximation to the scattered field in (2.34) is $u^{\mathrm{s}}_{(N',N)}$, which is computed similarly, using the T-matrix with $E^{\infty}_{\boldsymbol{\ell}'}$ in (2.46) replaced with $E_{\boldsymbol{\ell}'}$.

3. Convergence analysis with parameter estimates

In this section we prove exponential convergence of the approximate online output far field computed using the offline-based T-matrix, truncated using an *a priori* bound on its size. The *a priori* bound depends only on the wavenumber and diameter of the scatterer and is independent of the shape of the scatterer. The main result is Theorem 3.5 which establishes an error bound for the approximate far field induced by an incident field in the space $X_{\boldsymbol{w}}$. This error bound can be computed explicitly in the case of incident plane waves or point-source incidence by analysing the regularity of each of these classes of incident field. Such specific error bounds are given in Sections 3.1 and 3.2, respectively.

In more detail, in this section we prove that $u^{\infty}_{(N',N)}$ converges exponentially to u^{∞} in $L^2(\mathbb{S}^{d-1})$ with respect to the truncation parameters N, N'.

LEMMA 3.1 Let $u^{\mathrm{inc}} \in X_{\boldsymbol{w}}$. Then

$$\begin{aligned}&\left\|u^{\infty}-u^{\infty}_{(N',N)}\right\|^2_{L^2(\mathbb{S}^{d-1})}\\&\quad\leqslant \left\|u^{\mathrm{inc}}\right\|^2_{X_{\boldsymbol{w}}}\left\{\sum_{\boldsymbol{\ell}\in\mathbb{I}_d}\frac{1}{w_{\boldsymbol{\ell}}}\left\|S^{\infty}\widetilde{E}_{\boldsymbol{\ell}}-S^{\infty}_{N'}\widetilde{E}_{\boldsymbol{\ell}}\right\|^2_{L^2(\mathbb{S}^{d-1})}+\sum_{\boldsymbol{\ell}\in\mathbb{I}_d\setminus\mathbb{I}_{d,N}}\frac{1}{w_{\boldsymbol{\ell}}}\left\|S^{\infty}\widetilde{E}_{\boldsymbol{\ell}}\right\|^2_{L^2(\mathbb{S}^{d-1})}\right\},\end{aligned}\tag{3.1}$$

where $S^{\infty}_{N'}\widetilde{E}_{\boldsymbol{\ell}}$ is the $L^2(\mathbb{S}^{d-1})$ orthogonal projection of $S^{\infty}\widetilde{E}_{\boldsymbol{\ell}}$ onto span $\{Y_{\boldsymbol{\ell}'}:\boldsymbol{\ell}'\in\mathbb{I}_{d,N'}\}$.

Proof. Using (2.42) and (2.46),

$$u^{\infty}-u^{\infty}_{(N',N)}=\sum_{\boldsymbol{\ell}'\in\mathbb{I}_d\setminus\mathbb{I}_{d,N'}}\left[\sum_{\boldsymbol{\ell}\in\mathbb{I}_d}t_{\boldsymbol{\ell}',\boldsymbol{\ell}}p_{\boldsymbol{\ell}}\right]Y_{\boldsymbol{\ell}'}+\sum_{\boldsymbol{\ell}'\in\mathbb{I}_{d,N'}}\left[\sum_{\boldsymbol{\ell}\in\mathbb{I}_d\setminus\mathbb{I}_{d,N}}t_{\boldsymbol{\ell}',\boldsymbol{\ell}}p_{\boldsymbol{\ell}}\right]Y_{\boldsymbol{\ell}'}.\tag{3.2}$$

Hence, by the orthonormality of the basis functions $Y_{\boldsymbol{\ell}'}$ of $L^2(\mathbb{S}^{d-1})$,

$$\left\|u^{\infty}-u^{\infty}_{(N',N)}\right\|^2_{L^2(\mathbb{S}^{d-1})}=\sum_{\boldsymbol{\ell}'\in\mathbb{I}_d\setminus\mathbb{I}_{d,N'}}\left|\sum_{\boldsymbol{\ell}\in\mathbb{I}_d}\frac{t_{\boldsymbol{\ell}',\boldsymbol{\ell}}}{\sqrt{w_{\boldsymbol{\ell}}}}\sqrt{w_{\boldsymbol{\ell}}}p_{\boldsymbol{\ell}}\right|^2+\sum_{\boldsymbol{\ell}'\in\mathbb{I}_{d,N'}}\left|\sum_{\boldsymbol{\ell}\in\mathbb{I}_d\setminus\mathbb{I}_{d,N}}\frac{t_{\boldsymbol{\ell}',\boldsymbol{\ell}}}{\sqrt{w_{\boldsymbol{\ell}}}}\sqrt{w_{\boldsymbol{\ell}}}p_{\boldsymbol{\ell}}\right|^2.\tag{3.3}$$

Hence, the Cauchy–Schwarz inequality and (2.27) yield

$$\begin{aligned}\left\|u^{\infty}-u^{\infty}_{(N',N)}\right\|^2_{L^2(\mathbb{S}^{d-1})}&\leqslant\left\|u^{\mathrm{inc}}\right\|^2_{X_{\boldsymbol{w}}}\left[\sum_{\boldsymbol{\ell}'\in\mathbb{I}_d\setminus\mathbb{I}_{d,N'}}\sum_{\boldsymbol{\ell}\in\mathbb{I}_d}\frac{|t_{\boldsymbol{\ell}',\boldsymbol{\ell}}|^2}{w_{\boldsymbol{\ell}}}+\sum_{\boldsymbol{\ell}'\in\mathbb{I}_{d,N'}}\sum_{\boldsymbol{\ell}\in\mathbb{I}_d\setminus\mathbb{I}_{d,N}}\frac{|t_{\boldsymbol{\ell}',\boldsymbol{\ell}}|^2}{w_{\boldsymbol{\ell}}}\right]\\&=\left\|u^{\mathrm{inc}}\right\|^2_{X_{\boldsymbol{w}}}\left[\sum_{\boldsymbol{\ell}\in\mathbb{I}_d}\frac{1}{w_{\boldsymbol{\ell}}}\sum_{\boldsymbol{\ell}'\in\mathbb{I}_d\setminus\mathbb{I}_{d,N'}}|t_{\boldsymbol{\ell}',\boldsymbol{\ell}}|^2+\sum_{\boldsymbol{\ell}\in\mathbb{I}_d\setminus\mathbb{I}_{d,N}}\frac{1}{w_{\boldsymbol{\ell}}}\sum_{\boldsymbol{\ell}'\in\mathbb{I}_d}|t_{\boldsymbol{\ell}',\boldsymbol{\ell}}|^2\right]\\&=\left\|u^{\mathrm{inc}}\right\|^2_{X_{\boldsymbol{w}}}\left[\sum_{\boldsymbol{\ell}\in\mathbb{I}_d}\frac{1}{w_{\boldsymbol{\ell}}}\sum_{\boldsymbol{\ell}'\in\mathbb{I}_d\setminus\mathbb{I}_{d,N'}}|t_{\boldsymbol{\ell}',\boldsymbol{\ell}}|^2+\sum_{\boldsymbol{\ell}\in\mathbb{I}_d\setminus\mathbb{I}_{d,N}}\frac{1}{w_{\boldsymbol{\ell}}}\left\|S^{\infty}\widetilde{E}_{\boldsymbol{\ell}}\right\|^2_{L^2(\mathbb{S}^{d-1})}\right],\end{aligned}$$

where in the last line we used (2.40). Now the result (3.1) follows from using

$$(S^{\infty}_{N'}\widetilde{E}_{\boldsymbol{\ell}})(\widehat{\boldsymbol{x}})=\sum_{\boldsymbol{\ell}'\in\mathbb{I}_{d,N'}}t_{\boldsymbol{\ell}',\boldsymbol{\ell}}Y_{\boldsymbol{\ell}'}(\widehat{\boldsymbol{x}}),\qquad\widehat{\boldsymbol{x}}\in\mathbb{S}^{d-1},\tag{3.4}$$

and the identity

$$\left\|S^{\infty}\widetilde{E}_{\boldsymbol{\ell}}-S^{\infty}_{N'}\widetilde{E}_{\boldsymbol{\ell}}\right\|^2_{L^2(\mathbb{S}^{d-1})}=\sum_{\boldsymbol{\ell}'\in\mathbb{I}_d\setminus\mathbb{I}_{d,N'}}|t_{\boldsymbol{\ell}',\boldsymbol{\ell}}|^2.\tag{3.5}$$

□

Next we estimate the first term in (3.1). We recall that ρ_D is the radius of the scatterer D, that $R > \rho_D$ is fixed and that k is the wavenumber of the obstacle scattering problem.

LEMMA 3.2 The restrictions of the incident base fields from (2.15) satisfy

$$\left\|\widetilde{E}_{\boldsymbol{\ell}}\restriction_{\partial D}\right\|_{Z(\partial D)} \leqslant C\left(\frac{\rho_D}{R}\right)^{|\boldsymbol{\ell}|} \cdot \begin{cases} |\boldsymbol{\ell}|^{d/4-1/2} & \text{for a sound-soft scatterer,} \\ 1 & \text{for boundary conditions (2.3) and (2.4).} \end{cases}$$

Proof. The estimate is an immediate consequence of the bounds (2.16) and (2.17) from Lemma 2.1 and the standard interpolation estimate $\|u\|_{H^{1/2}(\partial D)} \leqslant C\,\|u\|^{1/2}_{H^1(\partial D)}\,\|u\|^{1/2}_{L^2(\partial D)}$. □

LEMMA 3.3 For all $\boldsymbol{\ell} \in \mathbb{I}_d$, and assuming the threshold condition $N' > Rk/2$, we have the estimate

$$\left\|S^\infty \widetilde{E}_{\boldsymbol{\ell}} - S^\infty_{N'}\widetilde{E}_{\boldsymbol{\ell}}\right\|^2_{L^2(\mathbb{S}^{d-1})} = \sum_{\boldsymbol{\ell}'\in\mathbb{I}_d\setminus\mathbb{I}_{d,N'}} |t_{\boldsymbol{\ell}',\boldsymbol{\ell}}|^2 \leqslant C\left(\frac{Rke}{2N'}\right)^{2N'}\left(\frac{\rho_D}{R}\right)^{2|\boldsymbol{\ell}|}|\boldsymbol{\ell}|^{d/2-1}. \tag{3.6}$$

Proof. We introduce the operators $S_R : Z(\partial D) \mapsto L^2(\partial B_R)$, $S_R g := u\restriction_{\partial B_R}$, where $u \in H^1_{\mathrm{loc}}(\mathbb{R}^d \setminus \overline{\Omega})$ is the solution of one of the exterior boundary value problems from (2.35) to (2.37). Obviously, S_R is a bounded linear operator. We denote by $\|S_R\|$ the norm of S_R as a mapping $Z(\partial D) \mapsto L^2(\partial B_R)$. This norm may be incorporated into constants, whenever appropriate.

Following the considerations in Colton & Kress (1998, Section 2.5) for $d = 3$ and in Kirsch (1986, Section 4) for $d = 2$, we find that the coefficients $a_{\boldsymbol{\ell}'}$ of the expansion (2.12) of u^∞, which is the far-field pattern of the solution u induced by the boundary data g, satisfy

$$\sum_{\boldsymbol{\ell}'\in\mathbb{I}_d}\left(\frac{2|\boldsymbol{\ell}'|}{Rke}\right)^{2|\boldsymbol{\ell}'|}|a_{\boldsymbol{\ell}'}|^2 \leqslant C(Rk)^{1-d}\,\|u\|^2_{L^2(\partial B_R)} \leqslant C(Rk)^{1-d}\,\|S_R\|\,\|g\|_{Z(\partial D)}\,. \tag{3.7}$$

Thus, defining the Hilbert space

$$Y_R = \left\{\psi = \sum_{\boldsymbol{\ell}'\in\mathbb{I}_d} g_{\boldsymbol{\ell}'}Y_{\boldsymbol{\ell}'} : \sum_{\boldsymbol{\ell}'\in\mathbb{I}_d}\left(\frac{2|\boldsymbol{\ell}'|}{Rke}\right)^{2|\boldsymbol{\ell}'|}|g_{\boldsymbol{\ell}'}|^2 < \infty\right\} \subset L^2(\mathbb{S}^{d-1}), \tag{3.8}$$

equipped with norm $\|\psi\|^2_{Y_R} = \sum_{\boldsymbol{\ell}'\in\mathbb{I}_d}\left(\frac{2|\boldsymbol{\ell}'|}{Rke}\right)^{2|\boldsymbol{\ell}'|}|g_{\boldsymbol{\ell}}|^2$, we find that $S^\infty_\partial : Z(\partial D) \to Y_R$ is a bounded linear operator. Note that the $t_{\boldsymbol{\ell}',\boldsymbol{\ell}}$ are the expansion coefficients of $S^\infty\widetilde{E}_{\boldsymbol{\ell}}$. Consequently, using (3.5),

$$\begin{aligned}\left\|S^\infty \widetilde{E}_{\boldsymbol{\ell}} - S^\infty_{N'}\widetilde{E}_{\boldsymbol{\ell}}\right\|^2_{L^2(\mathbb{S}^{d-1})} &= \sum_{\boldsymbol{\ell}'\in\mathbb{I}_d\setminus\mathbb{I}_{d,N'}}|t_{\boldsymbol{\ell}',\boldsymbol{\ell}}|^2 \\ &= \sum_{\boldsymbol{\ell}'\in\mathbb{I}_d\setminus\mathbb{I}_{d,N'}}\left(\frac{Rke}{2|\boldsymbol{\ell}'|}\right)^{2|\boldsymbol{\ell}'|}\left(\frac{2|\boldsymbol{\ell}'|}{Rke}\right)^{2|\boldsymbol{\ell}'|}|t_{\boldsymbol{\ell}',\boldsymbol{\ell}}|^2 \\ &= \sum_{\boldsymbol{\ell}'\in\mathbb{I}_d\setminus\mathbb{I}_{d,N'}} f_{Rke}(2|\boldsymbol{\ell}'|)\left(\frac{2|\boldsymbol{\ell}'|}{Rke}\right)^{2|\boldsymbol{\ell}'|}|t_{\boldsymbol{\ell}',\boldsymbol{\ell}}|^2,\end{aligned} \tag{3.9}$$

where for a fixed $a > 0$,

$$f_a(x) = (a/x)^x, \qquad x > 0. \tag{3.10}$$

It is easy to check that $\lim_{x\to 0} f_a(x) = 1$, that $\lim_{x\to\infty} f_a(x) = 0$, that $f_a(x)$ attains its maximum at $x^* = a/e$ and that $f_a(x)$ is a decreasing function for $x > x^*$. Using these properties in (3.9), for $N' > Rk/2$,

$$\begin{aligned}
\left\| S^\infty \widetilde{E}_{\boldsymbol{\ell}} - S^\infty_{N'} \widetilde{E}_{\boldsymbol{\ell}} \right\|^2_{L^2(\mathbb{S}^{d-1})} &\leqslant \left(\frac{Rke}{2N'}\right)^{2N'} \sum_{\boldsymbol{\ell}' \in \mathbb{I}_d \setminus \mathbb{I}_{d,N'}} \left(\frac{2|\boldsymbol{\ell}'|}{Rke}\right)^{2|\boldsymbol{\ell}'|} |t_{\boldsymbol{\ell}',\boldsymbol{\ell}}|^2 \\
&\leqslant \left(\frac{Rke}{2N'}\right)^{2N'} \left\| S^\infty \widetilde{E}_{\boldsymbol{\ell}} \right\|^2_{Y_R} \\
&\leqslant C \left(\frac{Rke}{2N'}\right)^{2N'} C \left\| S_R \right\| \left\| \widetilde{E}_{\boldsymbol{\ell}} \right\|^2_{Z(\partial D)} \\
&\leqslant C \left\| S_R \right\| \left(\frac{Rke}{2N'}\right)^{2N'} \left(\frac{\rho_D}{R}\right)^{2|\boldsymbol{\ell}|} |\boldsymbol{\ell}|^{d/2-1},
\end{aligned}$$

where in the last step we invoked the estimates of Lemma 3.2 and used a common upper bound. □

LEMMA 3.4 For all $R > \rho_D$ and $\boldsymbol{\ell} \in \mathbb{I}_d$,

$$\left\| S^\infty \widetilde{E}_{\boldsymbol{\ell}} \right\|^2_{L^2(\mathbb{S}^{d-1})} \leqslant C \left(\frac{\rho_D}{R}\right)^{2|\boldsymbol{\ell}|} |\boldsymbol{\ell}|^{d/2-1}. \tag{3.11}$$

Proof. Appealing to the continuity of $S^\infty_\partial : Z(\partial D) \mapsto L^2(\mathbb{S}^{d-1})$, the estimate is immediate from Lemma 3.2. □

Using (3.6) and (3.11) in (3.1), we get the following result.

THEOREM 3.5 Let $u^{\text{inc}} \in X_{\boldsymbol{w}}$. Assuming the threshold condition $N' > Rk/2$, there holds

$$\begin{aligned}
&\left\| u^\infty - u^\infty_{(N',N)} \right\|^2_{L^2(\mathbb{S}^{d-1})} \\
&\leqslant C \left\| u^{\text{inc}} \right\|^2_{X_{\boldsymbol{w}}} \left\{ \left(\frac{Rke}{2N'}\right)^{2N'} \sum_{\boldsymbol{\ell} \in \mathbb{I}_d} \frac{|\boldsymbol{\ell}|^{d/2-1}}{w_{\boldsymbol{\ell}}} \left(\frac{\rho_D}{R}\right)^{2|\boldsymbol{\ell}|} + \sum_{\boldsymbol{\ell} \in \mathbb{I}_d \setminus \mathbb{I}_{d,N}} \frac{|\boldsymbol{\ell}|^{d/2-1}}{w_{\boldsymbol{\ell}}} \left(\frac{\rho_D}{R}\right)^{2|\boldsymbol{\ell}|} \right\}.
\end{aligned} \tag{3.12}$$

3.1 *Convergence analysis for plane-wave incidence*

In this section we extend the error bound in Theorem 3.5 to the case of plane-wave incidence by analysing the regularity of the plane-wave incident field.

Let $u^{\text{inc}}(\boldsymbol{x}) = \exp(\mathrm{i}k\boldsymbol{x} \cdot \widehat{\boldsymbol{d}})$ be the plane wave with fixed incident direction $\widehat{\boldsymbol{d}}$ impinging on the obstacle $D \subseteq \mathbb{R}^d$ for $d = 2, 3$. The expansion coefficients of the incident wave in the expansion (2.27) are (Colton & Kress, 1998, Equation (3.66) for $d = 2$, Equation (2.45) for $d = 3$)

$$p_{\boldsymbol{\ell}} = \begin{cases} \sqrt{2\pi}\,\dfrac{\mathrm{i}^{|\boldsymbol{\ell}|}}{H^{(1)}_{|\boldsymbol{\ell}|}(kR)}\,\overline{Y_{\boldsymbol{\ell}}(\widehat{\boldsymbol{d}})} & \text{for } d = 2, \\ 4\pi\,\dfrac{\mathrm{i}^{|\boldsymbol{\ell}|}}{h^{(1)}_{|\boldsymbol{\ell}|}(kR)}\,\overline{Y_{\boldsymbol{\ell}}(\widehat{\boldsymbol{d}})} & \text{for } d = 3. \end{cases} \tag{3.13}$$

From (2.20), it is easy to see that the coefficients $p_{\boldsymbol{\ell}}$ satisfy the decay bound

$$|p_{\boldsymbol{\ell}}| \leqslant C \cdot \begin{cases} \dfrac{1}{H^{(1)}_{|\boldsymbol{\ell}|}(kR)}, & \text{for } d = 2 \\ \dfrac{|\boldsymbol{\ell}|^{1/2}}{h^{(1)}_{|\boldsymbol{\ell}|}(kR)}, & \text{for } d = 3 \end{cases} \qquad \boldsymbol{\ell} \in \mathbb{I}_d. \tag{3.14}$$

Hence, using the asymptotics of the Hankel and spherical Hankel functions for $|\boldsymbol{\ell}| \to \infty$ (Colton & Kress, 1998, Equations (3.58) and (2.39)), if we choose (see Fig. 2)

$$w_{\boldsymbol{\ell}} = |\boldsymbol{\ell}|^{-d} \left(\frac{2|\boldsymbol{\ell}|}{Rke}\right)^{2|\boldsymbol{\ell}|}, \tag{3.15}$$

it is easy to see that $u^{\mathrm{inc}} \in X_{\boldsymbol{w}}$. Also

$$\frac{|\boldsymbol{\ell}|^{d/2-1}}{w_{\boldsymbol{\ell}}} \left(\frac{\rho_D}{R}\right)^{2|\boldsymbol{\ell}|} = |\boldsymbol{\ell}|^{3d/2-1} \left(\frac{\rho_D ke}{2|\boldsymbol{\ell}|}\right)^{2|\boldsymbol{\ell}|} = g^{3d/2-1}_{Rke}(2|\boldsymbol{\ell}|) \left(\frac{\rho_D}{R}\right)^{2|\boldsymbol{\ell}|} \tag{3.16}$$

with

$$g^p_a(x) = \left(\frac{x}{2}\right)^p \left(\frac{a}{x}\right)^x, \qquad a, p > 0. \tag{3.17}$$

If we write $g^p_a(x) = \exp(\varphi(x))$, we see that the derivative $\varphi'(x)$ is a strictly decreasing function with $\varphi'(\frac{a}{e}) = \frac{ap}{e} > 0$ and $\varphi'(\frac{a}{e} + p) < 0$. Hence, $g^p_a(x)$ has a single global maximum at $x^*(a, p)$ with $x^*(a, p) \leqslant \frac{a}{e} + p$ (see Fig. 3). Thus, we obtain for $N > Rk/2 + \frac{3d}{4} - \frac{1}{2}$,

$$\sum_{\boldsymbol{\ell} \in \mathbb{I}_d \setminus \mathbb{I}_{d,N}} \frac{|\boldsymbol{\ell}|^{d/2-1}}{w_{\boldsymbol{\ell}}} \left(\frac{\rho_D}{R}\right)^{2|\boldsymbol{\ell}|} \leqslant g^{3d/2-1}_{Rke}(2N) \sum_{\boldsymbol{\ell} \in \mathbb{I}_d \setminus \mathbb{I}_{d,N}} \left(\frac{\rho_D}{R}\right)^{2|\boldsymbol{\ell}|} \leqslant C N^{3d/2-1} \left(\frac{Rke}{2N}\right)^{2N} \left(\frac{\rho_D}{R}\right)^{2N}. \tag{3.18}$$

The function $\varphi(x)$ introduced above is concave, increasing for $x \leqslant \frac{a}{e}$ and decreasing for $x \geqslant \frac{a}{e} + p$. It can be bounded by the minimum of the tangent lines at these two sites, which leads to the estimate $g^p_a(x) \leqslant (a/2)^p \exp(\frac{a}{e})$; cf. Fig. 3. From this we conclude that

$$\begin{aligned} \sum_{\boldsymbol{\ell} \in \mathbb{I}_d} \frac{|\boldsymbol{\ell}|^{d/2-1}}{w_{\boldsymbol{\ell}}} \left(\frac{\rho_D}{R}\right)^{2|\boldsymbol{\ell}|} &= \sum_{\boldsymbol{\ell} \in \mathbb{I}_d} g^{3d/2-1}_{Rke}(2|\boldsymbol{\ell}|) \left(\frac{\rho_D}{R}\right)^{2|\boldsymbol{\ell}|} \\ &\leqslant e^{Rk} (Rke/2)^{3d/2-1} \sum_{\boldsymbol{\ell} \in \mathbb{I}_d} \left(\frac{\rho_D}{R}\right)^{2|\boldsymbol{\ell}|} \leqslant C e^{Rk} (Rke/2)^{3d/2-1}. \end{aligned} \tag{3.19}$$

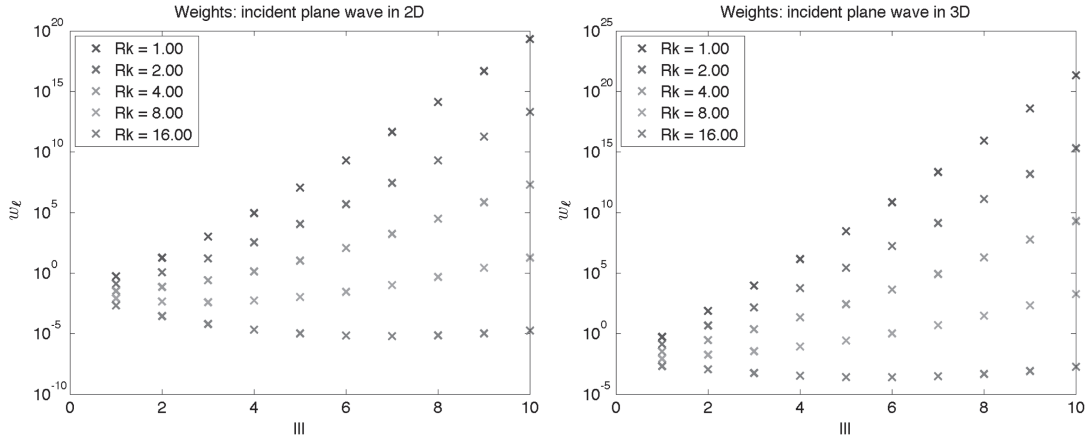

FIG. 2. The weights $w_{\boldsymbol{\ell}}$ from (3.15).

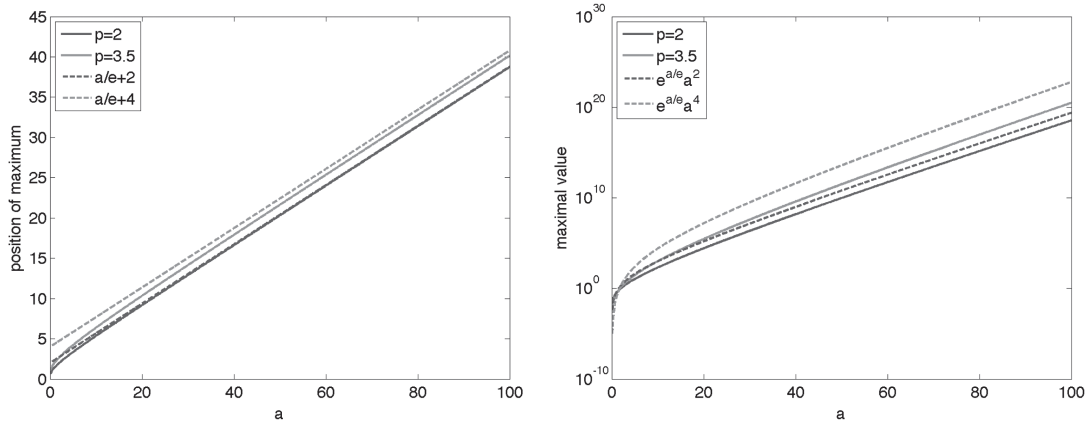

FIG. 3. $x^*(p,a)$ (left) and $g_a^p(x^*)$ (right) as functions of a for the relevant cases $p = 2, 3.5$.

Using (3.16), (3.18) and (3.19) in (3.12), we get the following exponential convergence of the far field obtained using the truncated T-matrix $T_{N',N}$.

THEOREM 3.6 Let $u^{\text{inc}}(\boldsymbol{x}) = \exp(\mathrm{i}k\boldsymbol{x}\cdot\widehat{\boldsymbol{d}})$, $\widehat{\boldsymbol{d}} \in \mathbb{S}^{d-1}$ for $d = 2, 3$. If the threshold conditions $N' > Rk/2$ and $N > Rk/2 + \frac{3d}{4} - \frac{1}{2}$ are satisfied, there holds the estimate

$$\left\| u^\infty - u^\infty_{(N',N)} \right\|^2_{L^2(\mathbb{S}^{d-1})} \leqslant C \left\{ e^{Rk} (Rke/2)^{3d/2-1} \left(\frac{Rke}{2N'} \right)^{2N'} + N^{3d/2-1} \left(\frac{\rho_D ke}{2N} \right)^{2N} \right\}. \tag{3.20}$$

3.2 *Convergence analysis for point-source incidence*

In this section we extend the error bound in Theorem 3.5 to the case of point-source incidence by analysing the regularity of the point-source induced incident field.

Let $\boldsymbol{x}_0 \in \mathbb{R}^d$ for $d = 2, 3$ with $|\boldsymbol{x}_0| > R$. Consider the incident field created by a point-source located at $\boldsymbol{x}_0$; that is,

$$u^{\text{inc}}(\boldsymbol{x}) = \begin{cases} H_0^{(1)}(k|\boldsymbol{x} - \boldsymbol{x}_0|), & d = 2, \\ \dfrac{\exp(\mathrm{i}k|\boldsymbol{x} - \boldsymbol{x}_0|)}{k|\boldsymbol{x} - \boldsymbol{x}_0|}, & d = 3. \end{cases} \tag{3.21}$$

The expansion coefficients of the incident wave in the expansion (2.27) are (Colton & Kress, 1998, Equation (3.65) for $d = 2$ and Equation (2.42) for $d = 3$)

$$p_{\boldsymbol{\ell}} = \begin{cases} \sqrt{2\pi}\, \dfrac{H_{|\boldsymbol{\ell}|}^{(1)}(k|\boldsymbol{x}_0|)}{H_{|\boldsymbol{\ell}|}^{(1)}(kR)} \overline{Y_{\boldsymbol{\ell}}(\widehat{\boldsymbol{x}}_0)} & \text{for } d = 2, \\ 4\pi\, \mathrm{i}k\, \dfrac{h_{|\ell|}^{(1)}(k|\boldsymbol{x}_0|)}{h_{|\boldsymbol{\ell}|}^{(1)}(kR)} \overline{Y_{\boldsymbol{\ell}}(\widehat{\boldsymbol{x}}_0)} & \text{for } d = 3, \end{cases} \qquad \boldsymbol{\ell} \in \mathbb{I}_d. \tag{3.22}$$

By (2.20) it is easy to see that the coefficients $p_{\boldsymbol{\ell}}$ satisfy the decay bounds

$$|p_{\boldsymbol{\ell}}| \leqslant C \cdot \begin{cases} \left| \dfrac{H_{|\boldsymbol{\ell}|}^{(1)}(k|\boldsymbol{x}_0|)}{H_{|\boldsymbol{\ell}|}^{(1)}(kR)} \right| & \text{for } d = 2, \\ |\boldsymbol{\ell}|^{1/2} \left| \dfrac{h_{|\boldsymbol{\ell}|}^{(1)}(k|\boldsymbol{x}_0|)}{h_{|\boldsymbol{\ell}|}^{(1)}(kR)} \right| & \text{for } d = 3, \end{cases} \qquad \boldsymbol{\ell} \in \mathbb{I}_d. \tag{3.23}$$

Hence, using the asymptotics of the Hankel and spherical Hankel functions for $|\boldsymbol{\ell}| \to \infty$, we arrive at the bound

$$|p_{\boldsymbol{\ell}}| \leqslant C|\boldsymbol{\ell}|^{d/2-1} \left(\frac{R}{|\boldsymbol{x}_0|} \right)^{|\boldsymbol{\ell}|}, \quad \boldsymbol{\ell} \in \mathbb{I}_d. \tag{3.24}$$

Thus, if we choose $w_0 := 1$ and

$$w_{\boldsymbol{\ell}} := \frac{1}{|\boldsymbol{\ell}|^d} \left(\frac{|\boldsymbol{x}_0|}{R} \right)^{2|\boldsymbol{\ell}|}, \qquad \boldsymbol{\ell} \in \mathbb{I}_d, \ \ |\boldsymbol{\ell}| > 0, \tag{3.25}$$

it is easy to see that $u^{\text{inc}} \in X_{\boldsymbol{w}}$ with $\left\| u^{\text{inc}} \right\|_{X_{\boldsymbol{w}}}$ bounded uniformly in $\boldsymbol{x}_0$ and k. In addition,

$$\frac{1}{w_{\boldsymbol{\ell}}} \left(\frac{\rho_D}{R} \right)^{2|\boldsymbol{\ell}|} |\boldsymbol{\ell}|^{d/2-1} = |\boldsymbol{\ell}|^{3d/2-1} \left(\frac{\rho_D}{|\boldsymbol{x}_0|} \right)^{2|\boldsymbol{\ell}|}, \tag{3.26}$$

which, using bounds for sums of the form $\sum_{k=N}^{\infty} k^p q^k$, $|q| < 1$, provides the estimates ($N > 1$)

$$\sum_{\boldsymbol{\ell} \in \mathbb{I}_d \setminus \mathbb{I}_{d,N}} \frac{1}{w_{\boldsymbol{\ell}}} \left(\frac{\rho_D}{R} \right)^{2|\boldsymbol{\ell}|} |\boldsymbol{\ell}|^{d/2-1} \leqslant C \left(\frac{\rho_D}{|\boldsymbol{x}_0|} \right)^{2N} \cdot \begin{cases} \dfrac{N^2}{(1 - (\rho_D/|\boldsymbol{x}_0|)^2)^3} & \text{for } d = 2, \\ \dfrac{N^{4.5}}{(1 - (\rho_D/|\boldsymbol{x}_0|)^2)^{5.5}} & \text{for } d = 3. \end{cases} \tag{3.27}$$

Using (3.27) and $\rho_D < R < |\boldsymbol{x}_0|$ in (3.12) of Theorem 3.5, we get the following exponential convergence of the far-field approximation obtained using the truncated T-matrix $T_{N',N}$.

THEOREM 3.7 Let u^{inc} be as in (3.21) with $|\boldsymbol{x}_0| > R$. Under the threshold condition $N' > Rk/2$,

$$\left\| u^\infty - u^\infty_{(N',N)} \right\|^2_{L^2(\mathbb{S}^{d-1})} \leqslant \frac{C}{(1-(\rho_D/|\boldsymbol{x}_0|)^2)^{q+1}} \left\{ \left(\frac{Rke}{2N'}\right)^{2N'} + N^q \left(\frac{\rho_D}{|\boldsymbol{x}_0|}\right)^{2N} \right\}, \tag{3.28}$$

with $q = 2$ for $d = 2$ and $q = 4.5$ for $d = 3$.

Note that the inevitable blow-up as the point-source approaches D is reflected in the estimate (3.28).

3.3 *Convergence analysis with approximate far fields*

The analysis above is based on the assumption that the far-field $S^\infty \widetilde{E}_{\boldsymbol{\ell}}$ required to construct the entries $t_{\boldsymbol{\ell}',\boldsymbol{\ell}}$ for $\boldsymbol{\ell}' \in \mathbb{I}_{d,N'}$ and $\boldsymbol{\ell} \in \mathbb{I}_{d,N}$ in (2.41) for the reduced basis T-matrix can be computed exactly. In practice, the computation of $S^\infty \widetilde{E}_{\boldsymbol{\ell}}$ requires numerical algorithms to solve (offline) the wave propagation model (2.1)–(2.5) with $u^{\text{inc}} = \widetilde{E}_{\boldsymbol{\ell}}$. In our approach, any numerical method (such as the finite element, boundary element, spectral or fundamental solution methods) can be used to solve the model. In this section, we complete our analysis by establishing bounds on the error in the far field obtained using a numerically computed T-matrix.

Let $0 < \epsilon(\boldsymbol{\ell}) < 1$ be the relative approximation error in the numerically computed far field with $u^{\text{inc}} = \widetilde{E}_{\boldsymbol{\ell}},\ \boldsymbol{\ell} \in \mathbb{I}_{d,N}$. That is, we assume that the numerical method is such that the numerical far-field $S^\infty_h \widetilde{E}_{\boldsymbol{\ell}}$ approximating $S^\infty \widetilde{E}_{\boldsymbol{\ell}}$ satisfies

$$\left\| S^\infty_h \widetilde{E}_{\boldsymbol{\ell}} - S^\infty \widetilde{E}_{\boldsymbol{\ell}} \right\|_{L^2(\mathbb{S}^{d-1})} \leqslant \epsilon(\boldsymbol{\ell}) \leqslant \epsilon, \quad \boldsymbol{\ell} \in \mathbb{I}_{d,N}. \tag{3.29}$$

A different S^∞_h may be employed for different incident fields $\widetilde{E}_{\boldsymbol{\ell}}$, to obtain a fixed accuracy $0 < \epsilon < 1$ so that $\epsilon(\boldsymbol{\ell}) \leqslant \epsilon,\ \boldsymbol{\ell} \in \mathbb{I}_{d,N}$.

Let $t_{\boldsymbol{\ell}',\boldsymbol{\ell},h}$ and $u^\infty_{(N',N,h)}$ be the associated approximations to $t_{\boldsymbol{\ell}',\boldsymbol{\ell}}$ and $u^\infty_{(N',N)}$, respectively. That is, based on (2.41) and (2.46), we have

$$t_{\boldsymbol{\ell}',\boldsymbol{\ell}} = \langle S^\infty \widetilde{E}_{\boldsymbol{\ell}}, Y_{\boldsymbol{\ell}'} \rangle, \qquad t_{\boldsymbol{\ell}',\boldsymbol{\ell},h} = \langle S^\infty_h \widetilde{E}_{\boldsymbol{\ell}}, Y_{\boldsymbol{\ell}'} \rangle, \qquad \boldsymbol{\ell}' \in \mathbb{I}_{d,N'},\ \boldsymbol{\ell} \in \mathbb{I}_{d,N}. \tag{3.30}$$

$$u^\infty_{(N',N)} = \sum_{\boldsymbol{\ell}' \in \mathbb{I}_{d,N'}} \left[\sum_{\boldsymbol{\ell} \in \mathbb{I}_{d,N}} t_{\boldsymbol{\ell}',\boldsymbol{\ell}} p_{\boldsymbol{\ell}} \right] Y_{\boldsymbol{\ell}'}, \qquad u^\infty_{(N',N,h)} = \sum_{\boldsymbol{\ell}' \in \mathbb{I}_{d,N'}} \left[\sum_{\boldsymbol{\ell} \in \mathbb{I}_{d,N}} t_{\boldsymbol{\ell}',\boldsymbol{\ell},h} p_{\boldsymbol{\ell}} \right] Y_{\boldsymbol{\ell}'}. \tag{3.31}$$

Using (3.30) and (3.29), we get

$$\sum_{\boldsymbol{\ell}' \in \mathbb{I}_{d,N'}} |t_{\boldsymbol{\ell}',\boldsymbol{\ell},h} - t_{\boldsymbol{\ell}',\boldsymbol{\ell}}|^2 \leqslant \sum_{\boldsymbol{\ell}' \in \mathbb{I}_{d,N'}} \left| \left\langle \left(S^\infty_h - S^\infty \right) \widetilde{E}_{\boldsymbol{\ell}}, Y_{\boldsymbol{\ell}'} \right\rangle \right|^2 = \epsilon(\boldsymbol{\ell})^2. \tag{3.32}$$

Again using the $L^2(\mathbb{S}^{d-1})$ orthonormality of the $Y_{\boldsymbol{\ell}'}$, (3.31) and (3.32), we get

$$\left\|u^{\infty}_{(N',N,h)} - u^{\infty}_{(N',N)}\right\|^2_{L^2(\mathbb{S}^{d-1})} \leqslant \sum_{\boldsymbol{\ell}\in\mathbb{I}_{d,N}} \sum_{\boldsymbol{\ell}'\in\mathbb{I}_{d,N'}} |t_{\boldsymbol{\ell}',\boldsymbol{\ell},h} - t_{\boldsymbol{\ell}',\boldsymbol{\ell}}|^2 \, |p_{\boldsymbol{\ell}}|^2$$

$$\leqslant \sum_{\boldsymbol{\ell}\in\mathbb{I}_{d,N}} w_{\boldsymbol{\ell}} \, |p_{\boldsymbol{\ell}}|^2 \sum_{\boldsymbol{\ell}'\in\mathbb{I}_{d,N'}} \frac{1}{w_{\boldsymbol{\ell}}} \left|t_{\boldsymbol{\ell}',\boldsymbol{\ell},h} - t_{\boldsymbol{\ell}',\boldsymbol{\ell}}\right|^2 \leqslant C \left\|u^{\mathrm{inc}}\right\|^2_{X_{\boldsymbol{w}}} \left\{ \sum_{\boldsymbol{\ell}\in\mathbb{I}_{d,N}} \frac{[\epsilon(\boldsymbol{\ell})]^2}{w_{\boldsymbol{\ell}}} \right\}. \quad (3.33)$$

Since

$$\left\|u^{\infty} - u^{\infty}_{(N',N,h)}\right\|^2_{L^2(\mathbb{S}^{d-1})} \leqslant 2 \left\|u^{\infty} - u^{\infty}_{(N',N)}\right\|^2_{L^2(\mathbb{S}^{d-1})} + 2 \left\|u^{\infty}_{(N',N,h)} - u^{\infty}_{(N',N)}\right\|^2_{L^2(\mathbb{S}^{d-1})},$$

Theorem 3.5 and (3.33) furnish the following result for the fully discrete reduced basis T-matrix method.

THEOREM 3.8 If $u^{\mathrm{inc}} \in X_w(\partial D)$ and $N' > Rk/2$,

$$\left\|u^{\infty} - u^{\infty}_{(N',N,h)}\right\|^2_{L^2(\mathbb{S}^{d-1})} \leqslant C \left\|u^{\mathrm{inc}}\right\|^2_{X_{\boldsymbol{w}}}$$

$$\times \left\{ \left(\frac{Rke}{2N'}\right)^{2N'} \sum_{\boldsymbol{\ell}\in\mathbb{I}_d} \frac{1}{w_{\boldsymbol{\ell}}} \left(\frac{\rho_D}{R}\right)^{2|\boldsymbol{\ell}|} |\boldsymbol{\ell}|^{d/2-1} + \sum_{\boldsymbol{\ell}\in\mathbb{I}_d\setminus\mathbb{I}_{d,N}} \frac{1}{w_{\boldsymbol{\ell}}} \left(\frac{\rho_D}{R}\right)^{2|\boldsymbol{\ell}|} |\boldsymbol{\ell}|^{d/2-1} + \sum_{\boldsymbol{\ell}\in\mathbb{I}_{d,N}} \frac{[\epsilon(\boldsymbol{\ell})]^2}{w_{\boldsymbol{\ell}}} \right\}. \quad (3.34)$$

For stable online computations, it is important to have a guaranteed accuracy for all offline computations; that is, $\epsilon(\boldsymbol{\ell}) \leqslant \epsilon$ for all $\boldsymbol{\ell} \in \mathbb{I}_{d,N}$. Henceforth, we assume this. Then, in the case of plane-wave incidence (see Section 3.1), by the definition (3.15) of the weights, we obtain analogously to (3.19)

$$\sum_{\boldsymbol{\ell}\in\mathbb{I}_{d,N}} \frac{1}{w_{\boldsymbol{\ell}}} \leqslant \sum_{\boldsymbol{\ell}\in\mathbb{I}_d} \left(\frac{Rke}{2|\boldsymbol{\ell}|}\right)^{2|\boldsymbol{\ell}|} |\boldsymbol{\ell}|^d \leqslant \sum_{j=1}^{\infty} \left(\frac{Rke}{2j}\right)^{2j} (2j)^{2d-2}$$

$$\leqslant \begin{cases} (Rke)^2 \sum\limits_{j=0}^{\infty} \left(\frac{Rke}{2j}\right)^{2j} & \text{for } d = 2, \\ 4(Rke)^2 + (Rke)^4 \sum\limits_{j=0}^{\infty} \left(\frac{Rke}{2j}\right)^{2j} & \text{for } d = 3, \end{cases}$$

$$\leqslant C \left((Rk)^2 + e^{Rk}(Rk)^{2d-2}\right), \quad (3.35)$$

where the bound on the infinite sum is derived from the integral of the function $g^0_a(x) = (\frac{a}{x})^x$. In Fig. 4 we demonstrate numerically that the bound (3.35) holds with $C = 10$. Estimates on the constant C could be derived by investigation of the upper bound of an integral of the function $g^0_a(x)$, but the calculations are lengthy and we skip such details.

Hence, from Theorem 3.8 in combination with Theorem 3.6, we get the following convergence result for the far field computed using the fully discrete reduced basis T-matrix $T_{N',N,h}$.

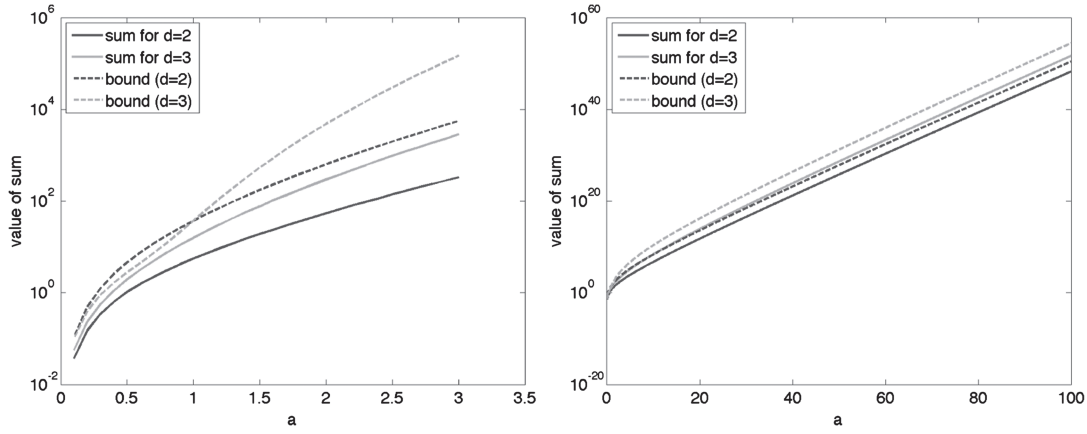

FIG. 4. Values of $\sum_{\boldsymbol{\ell}\in\mathbb{I}_d}\left(\frac{ae}{2|\boldsymbol{\ell}|}\right)^{2|\boldsymbol{\ell}|}|\boldsymbol{\ell}|^d$ with $a>0$ and bounds from (3.35) with $C=10$. The figure on the left shows the sum and bound for small a and is a magnification of the figure on the right.

THEOREM 3.9 Let $u^{\text{inc}}(\boldsymbol{x})=\exp(\mathrm{i}k\boldsymbol{x}\cdot\widehat{\boldsymbol{d}})$, $d=2,3$, and assume that $N'>Rk/2$ and $N>Rk/2+d-1$. Then

$$\left\|u^\infty-u^\infty_{(N',N,h)}\right\|^2_{L^2(\mathbb{S}^{d-1})}\leqslant C\left\{e^{Rk}(Rke/2)^{3d/2-1}\left(\frac{Rke}{2N'}\right)^{2N'}\right.$$
$$\left.+N^{3d/2-1}\left(\frac{\rho_D ke}{2N}\right)^{2N}+\left((Rk)^2+e^{Rk}(Rk)^{2d-1}\right)\epsilon^2\right\},\qquad(3.36)$$

with $C>0$ depending only on D and Rk.

In the case of point-source incidence (see Section 3.2) one finds that (cf. (3.27)),

$$\sum_{\boldsymbol{\ell}\in\mathbb{I}_{d,N}}\frac{1}{w_{\boldsymbol{\ell}}}\leqslant\sum_{\boldsymbol{\ell}\in\mathbb{I}_d}|\boldsymbol{\ell}|^d\left(\frac{R}{|\boldsymbol{x}_0|}\right)^{2|\boldsymbol{\ell}|}\leqslant\frac{C}{(1-(R/|\boldsymbol{x}_0|)^2)^{2d-1}}.\qquad(3.37)$$

Again using Theorem 3.8, for the point-source induced incident waves, we get the following convergence result for the far field computed using the fully discrete reduced basis T-matrix $T_{N',N,h}$.

THEOREM 3.10 For $d=2,3$, let u^{inc} be as in (3.21) with $|\boldsymbol{x}_0|>R$. For $N'>Rk/2$,

$$\left\|u^\infty-u^\infty_{(N',N,h)}\right\|^2_{L^2(\mathbb{S}^{d-1})}\leqslant\frac{C}{(1-(R/|\boldsymbol{x}_0|)^2)^{2d-1}}\left\{\left(\frac{Rke}{2N'}\right)^{2N'}+N^q\left(\frac{\rho_D}{|\boldsymbol{x}_0|}\right)^{2N}+\epsilon^2\right\},\qquad(3.38)$$

with $q=2$ for $d=2$, and $q=4.5$ for $d=3$.

4. Numerical results

In this section, we investigate numerically the estimates of Theorems 3.6 and 3.7 by showing exponential convergence of the simulated far field for several two- and three-dimensional sound-soft scatterers. For

each obstacle, we simulate scattering of incident plane waves and of waves originating from point-sources outside a ball of radius ρ_D circumscribing the scatterer.

Our three-dimensional obstacles are a sphere and a nonconvex obstacle that models an erythrocyte (a red blood cell, Wriedt *et al.*, 2006). Our two-dimensional obstacles are their two-dimensional cross-section or cross-sectional counterparts, namely, a circle and a peanut-shaped Cassini oval (Hellmers

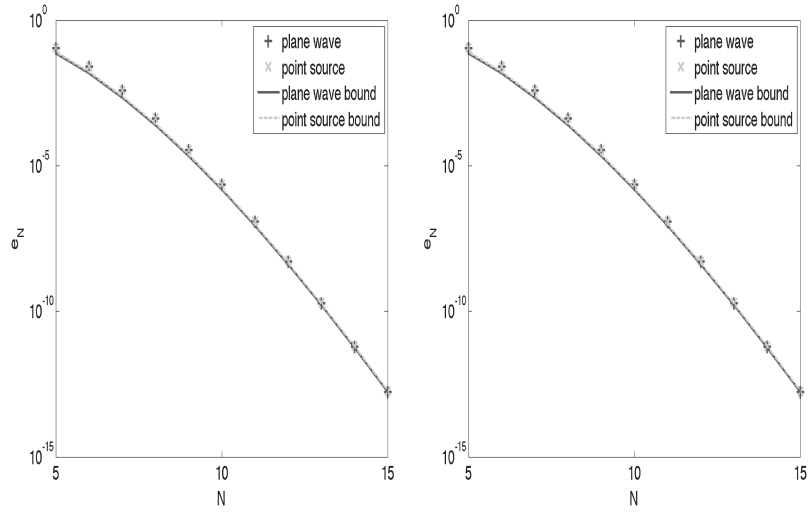

FIG. 5. The error e_N in (4.1) and theoretical bounds in (3.20) and (3.28) for plane-wave and point-source incidence (with $k = 10$) on a circle (left) and a sphere (right).

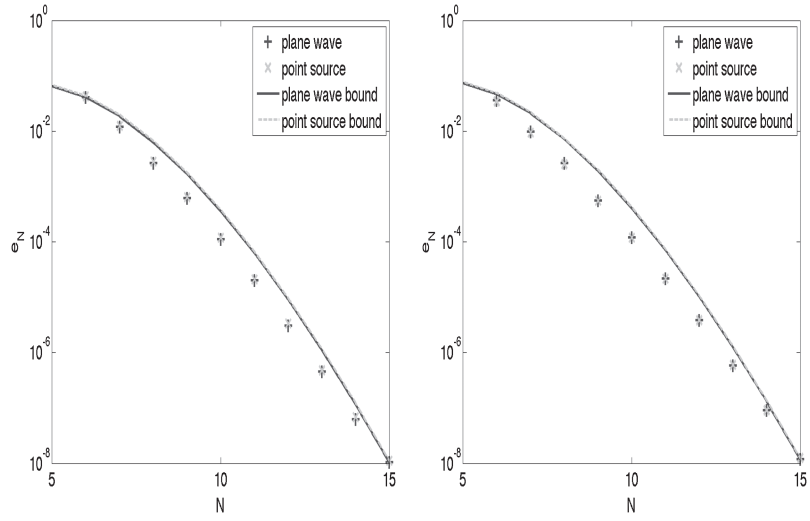

FIG. 6. The error e_N in (4.2) and theoretical bounds in (3.20) and (3.28) for plane-wave and point-source incidence (with $k = 10$) on a peanut (left) and an erythrocyte (right).

et al., 2006). All our scatterers are normalized so that they have unit diameter; that is, $\rho_D = 0.5$. In our point-source experiments, we chose $|\boldsymbol{x}_0| = 3$ so that $\rho_D/|\boldsymbol{x}_0| = 0.17$.

In all our experiments, for various parameter values $N' = N$, we first compute entries in the reduced basis truncated T-matrix $T_{N,N,h}$ using (3.30), with $S^{\infty}\widetilde{E}_{\boldsymbol{\ell}}$, $\boldsymbol{\ell} \in \mathbb{I}_d$, computed with high accuracy using the high-order algorithm in Ganesh & Graham (2004) for $d = 3$ and in Barnett & Betcke (2008) for $d = 2$. In order to demonstrate the exponential convergence of our reduced basis T-matrix algorithm,

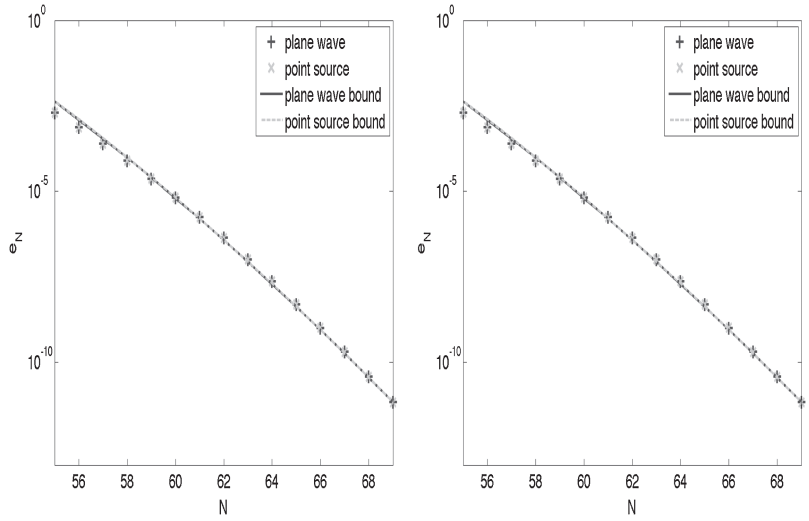

FIG. 7. The error e_N in (4.1) and theoretical bounds in (3.20) and (3.28) for plane-wave and point-source incidence (with $k = 100$) on a circle (left) and a sphere (right).

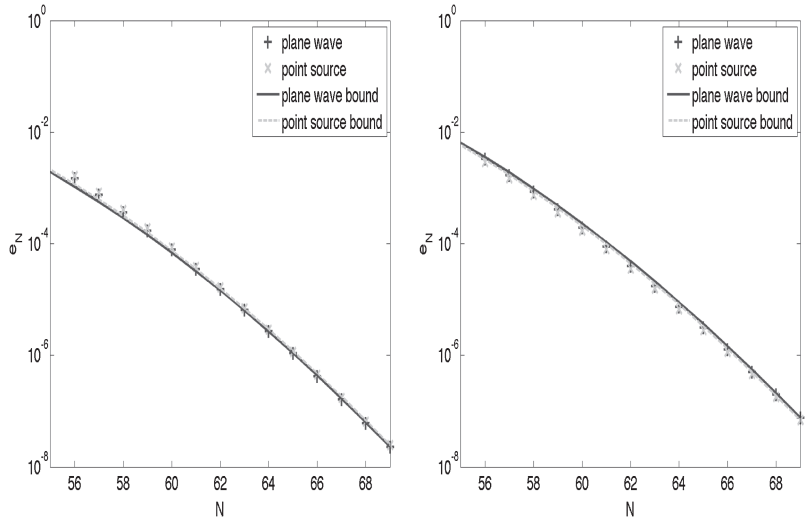

FIG. 8. The error e_N in (4.2) and theoretical bounds in (3.20) and (3.28) for plane-wave and point-source incidence (with $k = 100$) on a peanut (left) and an erythrocyte (right).

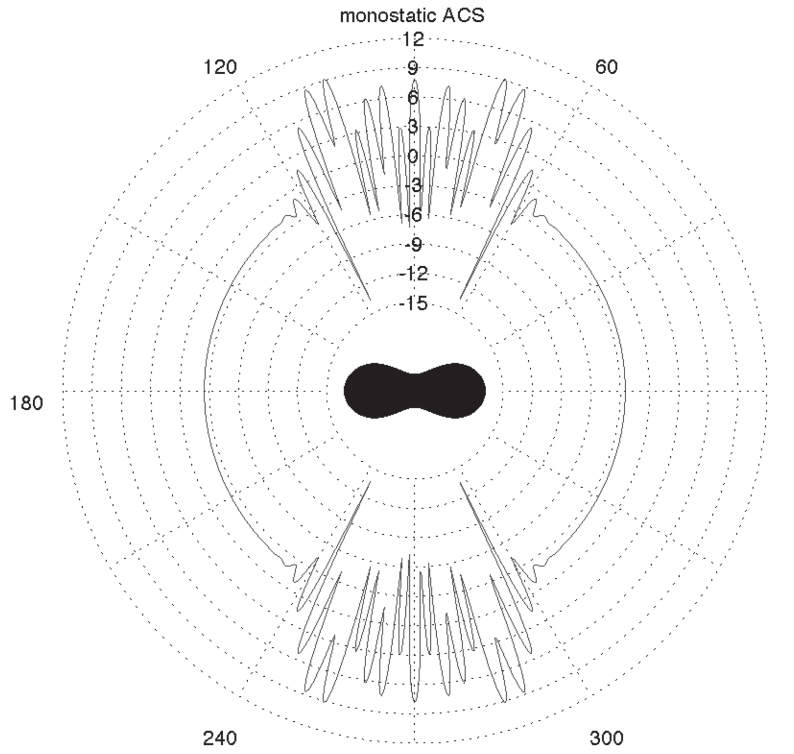

FIG. 9. The monostatic ACS of the Cassini oval (2D) for plane-wave incidence with $k = 100$.

the discretization parameters in these high-order algorithms were chosen, based on various experiments, so that ϵ in (3.29) is of the order 10^{-15} for the circle and sphere and 10^{-10} for the nonconvex obstacles. This ensures that for our experiments, the terms with $\epsilon^2 < 10^{-20}$ are much smaller than the other terms in (3.36) and (3.38) and, hence, we omit the index h.

Using $T_{N,N}$, we computed the approximate far-field $u^{\infty}_{(N,N)}$ via (3.31), and the scattered-field $u^{\mathrm{s}}_{(N',N)}$ with $E^{\infty}_{\boldsymbol{\ell}'}$ in (2.46) replaced with $E_{\boldsymbol{\ell}'}$.

For the circle and sphere obstacles, the far field induced by the incident plane wave or point-source is known analytically in (Mie) series form. Using the optimal truncation parameter given in Ganesh & Hawkins (2006) and Wiscombe (1990) (which depends on $k\rho_D$), we truncate the Mie series to very high accuracy and obtain the true far-field u^{∞}. Thus, for these obstacles we are able to compute the relative error,

$$e_N = \frac{\left\| u^{\infty} - u^{\infty}_{(N,N)} \right\|_{L^2(S^{d-1})}}{\|u^{\infty}\|_{L^2(\mathbb{S}^{d-1})}}, \tag{4.1}$$

in our approximation, $u^{\infty}_{(N,N,h)}$, to the true far-field u^{∞}.

The erythrocyte and Cassini oval scatterers are considered challenging obstacles for scattering simulations because they have nonconvex regions that give rise to multiple reflections. The scattered field for these scatterers is not known analytically. For these scatterers we demonstrate the convergence of

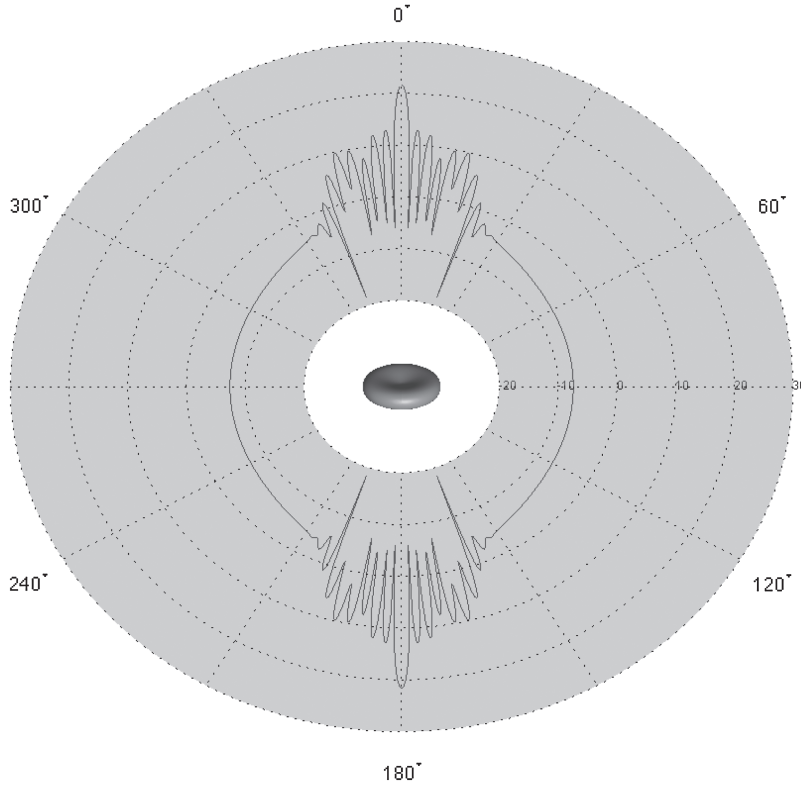

FIG. 10. The monostatic ACS of the erythrocyte (3D) for plane-wave incidence with $k = 100$.

the approximation, $u^{\infty}_{(N,N)}$, with respect to N by tabulating

$$e_N = \frac{\left\| u^{\infty}_{(M,M)} - u^{\infty}_{(N,N)} \right\|_{L^2(\mathbb{S}^{d-1})}}{\left\| u^{\infty}_{(M,M)} \right\|_{L^2(\mathbb{S}^{d-1})}}, \tag{4.2}$$

where $u^{\infty}_{(M,M)}$ is a reference solution, computed using the T-matrix with M fixed sufficiently large so that the reference solution is a highly accurate approximation to the exact far field. We approximate the $L_2(\mathbb{S}^{d-1})$ norms in (4.1) and (4.2) using Parseval's inequality. Using (3.13) and (3.22), it is easy to see that e_N in (4.1) and (4.2) is independent of the choice of R used in the theoretical analysis for estimating the errors in (3.20) and (3.28).

Values of e_N in Figs 5–8 substantiate the exponential convergence established in Theorems 3.6 and 3.7 for the plane-wave and point-source incidence, respectively, on a circle, sphere, peanut and erythrocyte with $k = 10, 100$. In addition, these figures demonstrate that the theoretical bounds are optimal for some appropriate choice of C and R in (3.20) and (3.28). For each plot in Figs 5–8, the constant C was obtained by fitting with the last data e_N, leading to an appropriate value R closely matching the experimental observation.

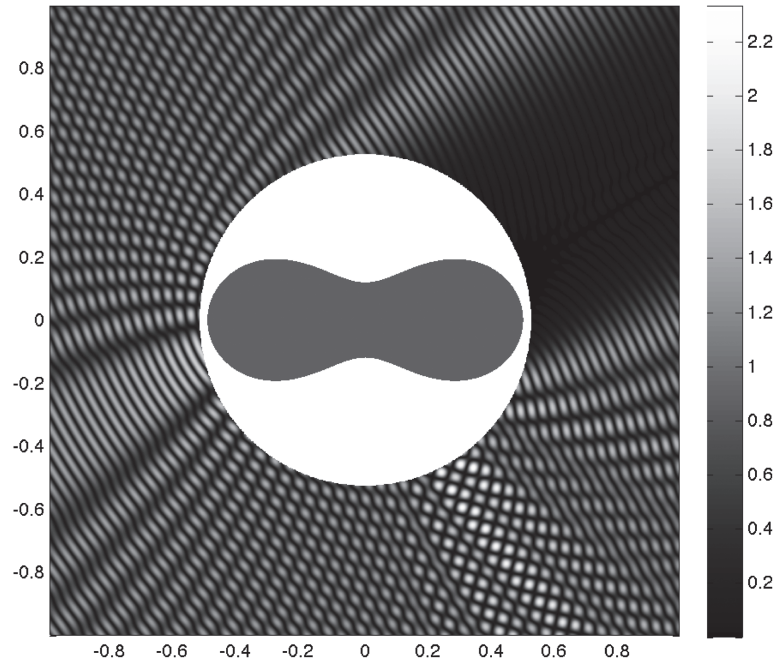

FIG. 11. The total exterior field of the Cassini oval (2D) for plane-wave incidence with $k = 100$.

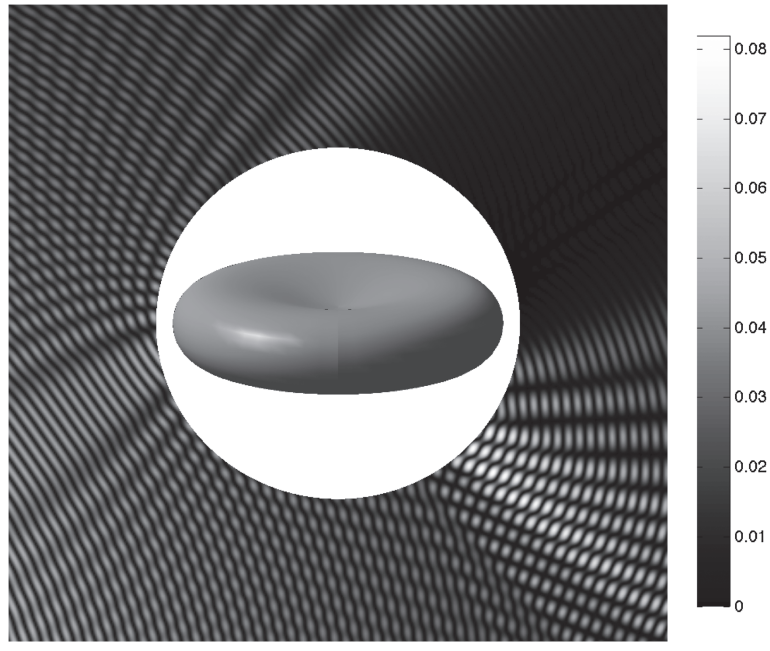

FIG. 12. The total exterior field of the erythrocyte (3D) for point-source incidence with $k = 100$.

One of the advantages of the offline computation and storage of the reduced basis T-matrix is the quick online computation of the ACS for many different incident fields. In particular, this is very useful to simulate the monostatic ACS, which requires thousands of incident directions. In Figs 9 and 10, we visualize our reduced basis T-matrix based monostatic ACS simulations for $k = 100$.

In Figs 11 and 12, for $k = 100$, we visualize the reduced basis T-matrix based total field outside the ball of radius $R = \rho_D + 0.05$ circumscribing the nonconvex obstacles of radius ρ_D for a plane wave (with incident direction $\boldsymbol{x}(\pi/6)$) impinging on the Cassini oval and a point-source (located at $-\boldsymbol{x}(5\pi/6, 0)$) induced incident wave impinging on the erythrocyte.

Acknowledgements

Part of this work was carried out while MG was a Forschunginstitute für Mathematik (FIM) guest at ETH Zurich. Support of the FIM and the Colorado Golden Energy Computing Organization (GECO) are gratefully acknowledged. Computations were carried out using the GECO cluster Ra.

REFERENCES

ABRAMOWITZ, M. & STEGUN, I. (1970) *Handbook of Mathematical Functions*. New York: Dover Publications.

AFONSO, S. M. B., LYRA, P. R. M., ALBUQUERQUE, T. M. M. & MOTTA, R. S. (2010) Structural analysis and optimization in the framework of reduced-basis method. *Struct. Multidisc. Optim.*, **40**, 177–199.

BARNETT, A. H. & BETCKE, T. (2008) Stability and convergence of the method of fundamental solutions for Helmholtz problems on analytic domains. *J. Comput. Phys.*, **227**, 7003–7026.

CHEN, Y., HESTHAVEN, J. S. & MADAY, Y. (2011) A seamless reduced basis element method for 2D Maxwell's problem: an introduction. *ICOSAHOM 2009 Proc.*, **76**, 141–152.

CHEN, Y., HESTHAVEN, J. S., MADAY, Y. & RODRIGUEZ, J. (2010) Certified reduced basis methods and output bounds for the harmonic Maxwell equations. *SIAM J. Sci. Comput.*, **32**, 970–996.

COLTON, D. & KRESS, R. (1998) *Inverse Acoustic and Electromagnetic Scattering Theory*. Berlin, Germany: Springer.

DOICU, A., WRIEDT, T. & EREMIN, Y. (2006) *Light Scattering by Systems of Particles. Null-Field Method with Discrete Sources—Theory and Programs*. Berlin, Germany: Springer.

FARES, B., HESTHAVEN, J., MADAY, Y. & STAMM, B. (2011) The reduced basis method for the electric field integral equation. *J. Comput. Phys.*, **230**, 5532–5555.

FREEDEN, W., GERVENS, T. & SCHREINER, M. (1998) *Constructive Approximation on the Sphere*. Oxford: Oxford University Press.

GANESH, M. & GRAHAM, I. G. (2004) A high-order algorithm for obstacle scattering in three dimensions. *J. Comput. Phys.*, **198**, 211–242.

GANESH, M. & HAWKINS, S. C. (2006) Improved high-order algorithms for Mie scattering. *WSEAS Trans. Math.*, **5**, 663–670.

GANESH, M. & HAWKINS, S. C. (2008) A far-field based T-matrix method for three dimensional acoustic scattering. *ANZIAM J.*, **50**, C121–C136.

GANESH, M. & HAWKINS, S. C. (2009) A far-field based T-matrix method for two dimensional obstacle scattering. *ANZIAM J.*, **51**, C201–C216.

GANESH, M., HESTHAVEN, J. S. & STAMM, B. (2011) A reduced basis method for multiple electromagnetic scattering in three dimensions (submitted for publication). Available at http://www.mines.edu/∼mganesh/RBM_multiple_final_submit.pdf.

HELLMERS, J., EREMINA, E. & WRIEDT, T. (2006) Simulation of light scattering by biconcave Cassini ovals using the nullfield method with discrete sources. *J. Opt. A: Pure Appl. Opt.*, **8**, 1–9.

KIRSCH, A. (1986) The denseness of the far field patterns for the transmission problem. *IMA J. Appl. Math.*, **37**, 213–225.

MARTIN, P. A. (2006) *Multiple Scattering: Interaction of Time-Harmonic Waves with N Obstacles*. Cambridge: Cambridge University Press.

MISHCHENKO, M. I., TRAVIS, L. D. & LACIS, A. A. (2006) *Multiple Scattering of Light by Particles: Radiative Transfer and Coherent Backscattering*. Cambridge: Cambridge University Press.

MISHCHENKO, M. I., TRAVIS, L. D. & MACKOWSKI, D. W. (1996) T-matrix computations of light scattering by nonspherical particles: a review. *J. Quant. Spectrosc. Radiat. Transfer*, **55**, 535–575.

PATERA, A. T. & ROZZA, G. (2011) *Reduced Basis Methods and A Posteriori Error Estimation for Parameterized Partial Differential Equations*. MIT Pappalardo Graduate Monographs in Mechanical Engineering (in press). Available at http://augustine.mit.edu/methodology/methodology_book.htm.

POMPLUN, J., BURGER, S., ZSCHIEDRICH, L. & SCHMIDT, F. (2011) Reduced basis method for real-time inverse scatterometry. *Proc. SPIE*, **8083**, 808308.

POMPLUN, J. & SCHMIDT, F. (2010) Accelerated a posteriori error estimation for the reduced basis method with application to 3D electromagnetic scattering problems. *SIAM J. Sci. Comput.*, **32**, 498–520.

WATERMAN, P. (1965) Matrix formulation of electromagnetic scattering. *Proc. IEEE*, **53**, 805–812.

WISCOMBE, W. J. (1990) Improved Mie scattering algorithms. *Appl. Opt.*, **19**, 1505–1509.

WRIEDT, T., HELLMERS, J., EREMINA, E. & SCHUH, R. (2006) Light scattering by single erythrocyte: comparison of different methods. *J. Quant. Spectrosc. Radiat. Transfer*, **100**, 444–456.